Low-Frequency Electromagnetic Energy Harvesting

by

Karim El-Rayes

A thesis
presented to the University of Waterloo
in fulfillment of the
thesis requirement for the degree of
Master of Applied Science
in
Electrical and Computer Engineering

Waterloo, Ontario, Canada, 2011

I hereby declare that I am the sole author of this thesis. This is a true copy of the thesis, including any required final revisions, as accepted by my examiners.
I understand that my thesis may be made electronically available to the public.

ABSTRACT

The demand for portable permanent sources of electrical energy increases every day to power portable or non-accessible devices. Energy harvesting from vibrations offers a non-traditional source of energy. It is renewable and prevailing, since nature around is rich in kinetic energy that can be harvested.

In this work, we have developed two mechanisms to harvest energy from low-frequency vibrations present in nature using electromagnetic transduction. The harvesting mechanisms use a mass-on-spring mechanical oscillator to capture kinetic energy from a host body. Prototypes embodying the two harvesting mechanisms were fabricated and tested. We identified the system parameters of the harvester prototypes and generated their frequency-response curves. We analyzed the results using and compared them with mathematical models of the system dynamics to characterize the harvesters' performance including their output power, center frequency, and harvesting bandwidth.

We were successful in demonstrating energy harvesters that can harvest low-frequency vibration with center frequencies in the range of 8-14 Hz, harvesting bandwidth in the range of 8-12Hz, and output power on the order of 1mW. The realized harvesters are relatively small, a few inches in dimension, and light, a few tens of grams in mass. We also introduced a novel electromagnetic transduction mechanism that can be used in harvesting low-frequency vibrations.

The novel electromagnetic transduction mechanism we developed induces a current in a coil by disrupting the electromagnetic field around the coil. where we have a coil wound around hollow track, a tube made of non-conducting material, surrounded by source of magnetic field, both coil and magnetic field source are stationary and a ball made of ferromagnetic material is moving freely along the tube cutting the field lines causing the magnetic field to be disrupted and induces current in the coil.

Acknowledgements

I would like to thank and acknowledge my mentors, friends and family who helped me through my study and work at the university of Waterloo, where I dedicate a special thanks to my supervisors Dr. Eihab Abdelrahman, Dr. Raafat Mansour and Dr. Ehab El-Saadany for their support and guidance during the program of study.

Also I would like to acknowledge and thank Dr. Carl Haas and Dr. Sebastian Fischmeister for many things I have learned from them during the projects and courses studied under their supervision.

I would like to thank my friends and colleagues Ahmed Abd-Elaziz, Ahmed Khalifa, Ayman Bahgat, Abdullatif Al-Wasel, Mahmoud Khater, and Mohamed Bendame for their support and fruitful discussions I had with them.

Dedication

To my parents... You inspired me with every step I have taken.

Contents

List of Figures

List of Tables

Chapter 1

Introduction

1.1 Motivation

"Energy", the keyword for today's global industry and economies, all people and all organizations are seeking for energy and all kinds of energy from any available resources, all scales of energy are required starting from powering small devices like cellphones or embedded pacemaker inside patient's body up to enormous amounts of energy required to light up a metropolitan like Toronto or New York. The focus of this thesis is harvesting or scavenging energy from physical phenomena that exist in the environment to power up low-power electronic devices to function and accomplish their tasks.

1.1.1 Energy Harvesting

Energy Harvesting is the process of capturing, scavenging, or hunting for energy from physical phenomena in nature, kinetic, solar, thermal ...etc, and converting it to electrical energy. Since energy is neither created nor destroyed, captured energy is either transformed to electrical energy or lost to various energy loss mechanisms, depending on the harvester design and the harvesting mechanism. The level of complexity of energy harvesting varies depends on five factors:

- The form of energy to be harvested and the amount of energy available in the

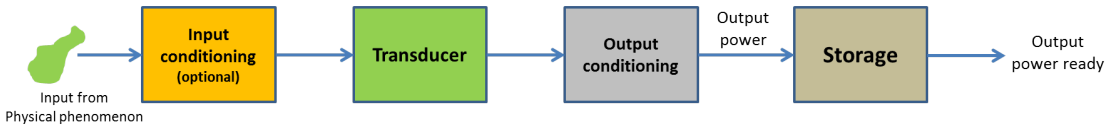

Figure 1.1: Phases of energy harvesting

environment.

- The technology used in harvesting and conversion as far as its reliability and suitability to the amount of energy being harvested, and efficiency.
- The type and design of the transducer.
- The need for input or output conditioning blocks, such asfilters, rectifiers, boosting circuits, and regulators.
- The type of energy storage element, since the output energy is not consumedin tandem with the conversion process.

Figure 1.1 summarizes the energy harvesting process phases and the importance of each phase.

1.1.2 Scales of energy harvesting

It is now common in daily life to find energy harvesters in use, some can convert and output relatively large amounts of electrical power that can feed the power like solar power stations and wind farms which can output up to hundreds of "Megawatts" of electrical power. On the other hand, small electronic devices requires a very low amount of energy to operate, some of these applications require a perpetual or sustainable source of energy depending on the device operating conditions and task, early examples of these devices are kinetic wrest watches and solar panel-powered calculators. Therefore, two categories of energy harvesters can be identified in terms of the level output power:

- Macro harvesting: generates high levels of electrical power on the order of a few hundreds of watts or more, that can feed the electrical grid like solar

power stations or wind farms. At this scale, energy harvesting units require mechanical and electrical component design, maintenance, and transmission lines and occupy large space.

- Micro harvesting: generates low levels of power (microwatts up to few watts). This category of harvesters is suitable to drive low power portable electronic devices, and applications that require a perpetual source of energy like RFID modules or wireless sensor networks, and sensors in hard to access places, where it is not feasible or practical to change batteries on a regular basis or to extend a power cable to them. This scale of energy harvesters has many advantages in terms of mechanical and electrical components' design simplicity, setup, maintenance, footprint, and size, integration with other systems and cost. On the other hand, the disadvantages of this category of energy harvesters are:

  - Intermittent output: since it harvests energy from the environment, the availability of output power depends on how frequent is the physical phenomenon being harvested.
  - Unregulated output: due to unpredictability of the output energy magnitude and frequency.
  - Very low output power: output power is low not just because the amount of energy being harvested is small, like that in human body motion or variation in air temperature, but also because of power losses in mechanical components and signal conditioning circuits.

Since micro-energy harvesters are used to scavenge micro-energy from a physical phenomenon, thermal, light, motion...etc, they should be highly sensitive and highly efficient by minimizing the losses as much as possible.

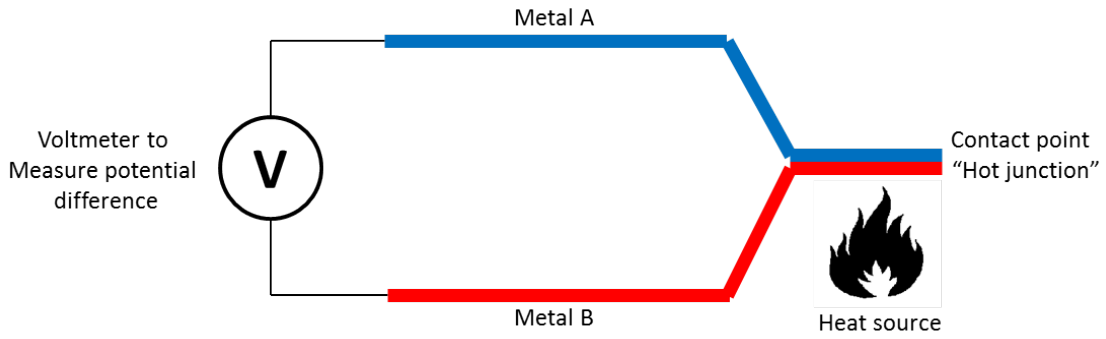

Figure 1.2: Basic thermocouple design

1.1.3 Micro Harvesting

In this section, techniques commonly deployed in micro-energy harvesting will be discussed. Three forms of energy are the most commonly harvested forms of energy due to the availability of legacy technology or to their high efficiency and abundance. These are:

- Thermal energy.
- Solar energy.
- Kinetic energy.
- Thermal energy is one of the most available sources of energy on earth found in air, human body, geothermal, and waste heat in fossil fuel based engines. The harvesting mechanism here is based on the “Seebeck effect” (thermocouple).The theory of operation of the thermocouple is that heating two metals in contact at one end will develop potential difference between at the end where they are not in contact Figure 1.2. Due to developments in the technology of semiconductors and chemical processing, the size and efficiency of energy harvesters based on this form of energy have improved significantly.
- Solar energy is the most commonly harvested form of energy using photovoltaic cells to convert light photons to electrical energy.

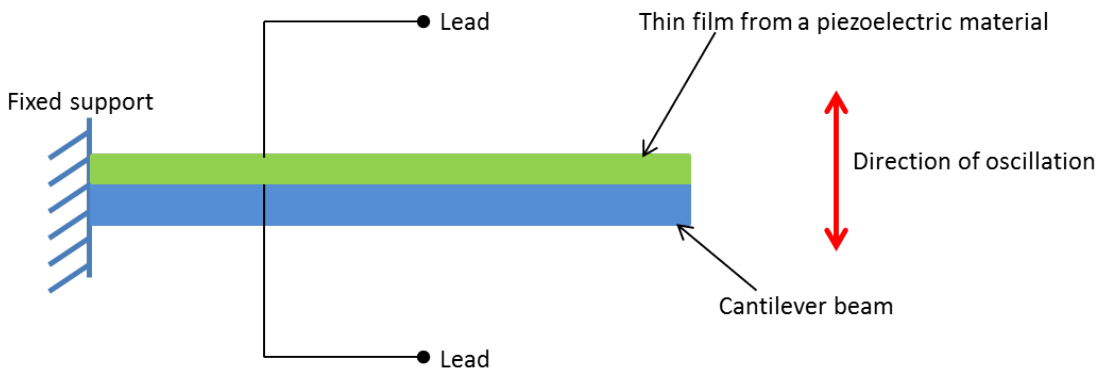

Figure 1.3: Basic design of a piezoelectric harvester

- Kinetic energy can be harvested from the motion rotary machines, mechanical vibrations, and impact events.

1.2 Energy harvesting transduction mechanisms from vibrations

This section discusses the transduction mechanisms used to convert mechanical vibrations to electrical energy.

1. Piezoelectric: Piezoelectric materials develop potential difference along the surface of material when exposed to strain, inversely; a piezoelectric material stimulated by an external potential difference undergoes strain. The structure of most energy harvester based on piezoelectric transduction involves a thin strip of piezoelectric material mounted on a simple cantilever beam exposed to vibrations, Figure 1.3. When the beam oscillates a potential difference develops along the opposite surfaces of the piezoelectric material. The output voltage amplitude is proportional to vibrations amplitude and the electromechanical coupling coefficients of the piezoelectric material. The output voltage of this kind of harvesters is relatively high which requires regulation using additional circuitry.

2. Electrostatic: This mechanism harvests accumulated charges between the two

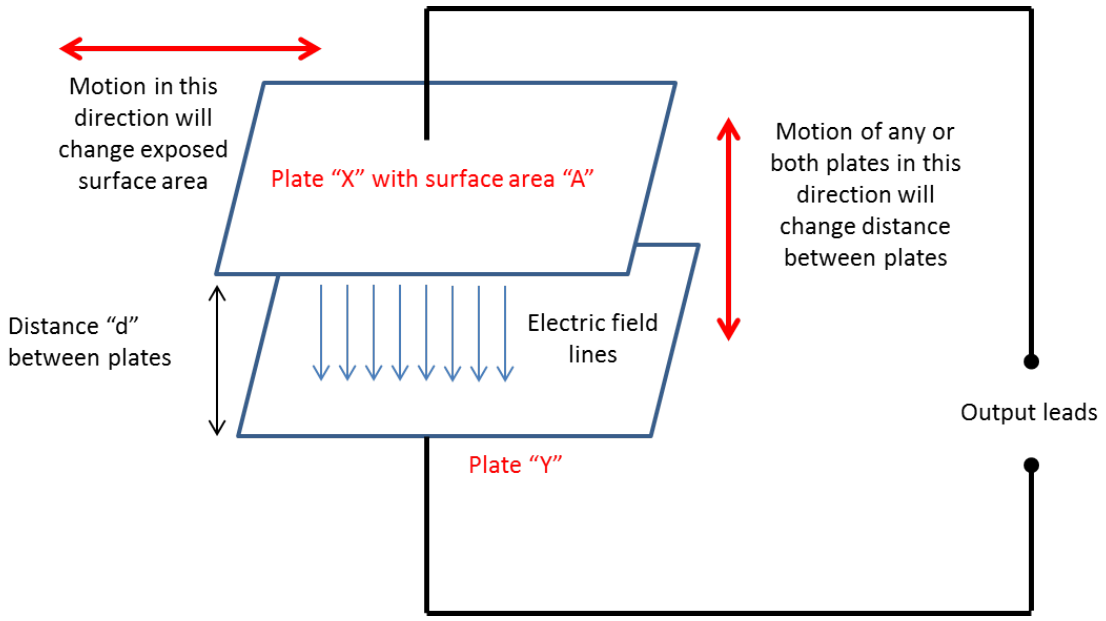

Figure 1.4: Basic idea of electrostatic energy harvesting

conducting plates of a variable capacitor as it changes its capacitance. Electrostatic harvesting exploits the proportional relationship between quantity of charges Q on the two plates and capacitance C when the potential difference V across the plates is held constant:

$$Q = CV_o \tag{1.1}$$

Capacitance is function of the surface area of the plates A exposed to each other and the separation distance d between them:

$$C = \epsilon_r \epsilon_o \frac{A}{d} \tag{1.2}$$

where $\epsilon_o = 8.854 \times 10^{-12} F/m$ is space permittivity and ϵ_r is the relative permittivity of the dielectric material between the two plates.

Figure 1.4 illustrates the ways in which variable capacitors harvest electrical energy. Captured kinetic energy moves one of the two plates horizontally to change the exposed surface area and therefore capacitance. As a result, charges Q are collected and harvested as kinetic energy keeps varying the

position of the capacitor plates. The same process can also be induced when kinetic energy is used to change the separation distance between the two plates. Electrostatic energy harvesters are designed to exploit either of these motion patterns.

3. Electromagnetic: Faraday's law of electromagnetic induction states that conductor moving across a magnetic field will developed potential difference between its terminals as it cuts the magnetic field lines. This transduction mechanism is based on using kinetic energy to create relative motion between a conducting wire and a magnetic field, Figure 1.5. The voltage generated across the conductor terminals V is proportional to the rate of change of the magnetic flux linkage ϕ.

$$V = -\frac{d\phi}{dt} \tag{1.3}$$

When a coil with N number of turns is used instead of a single turn conductor, the generated voltage in this case will be:

$$V = -N\frac{d\phi}{dt} \tag{1.4}$$

where ϕ in this case will be the average magnetic flux per coil turn. For electromagnetic harvesting, kinetic energy is used to change the relative position of the coil with respect to the magnetic field source which varies magnetic flux as a function of displacement. Therefore, the output voltage can be expressed as:

$$V = -N\frac{d\phi}{dt}\frac{dx}{dt} \tag{1.5}$$

where dx/dt is the rate of change of relative displacement, velocity, in the x-direction.

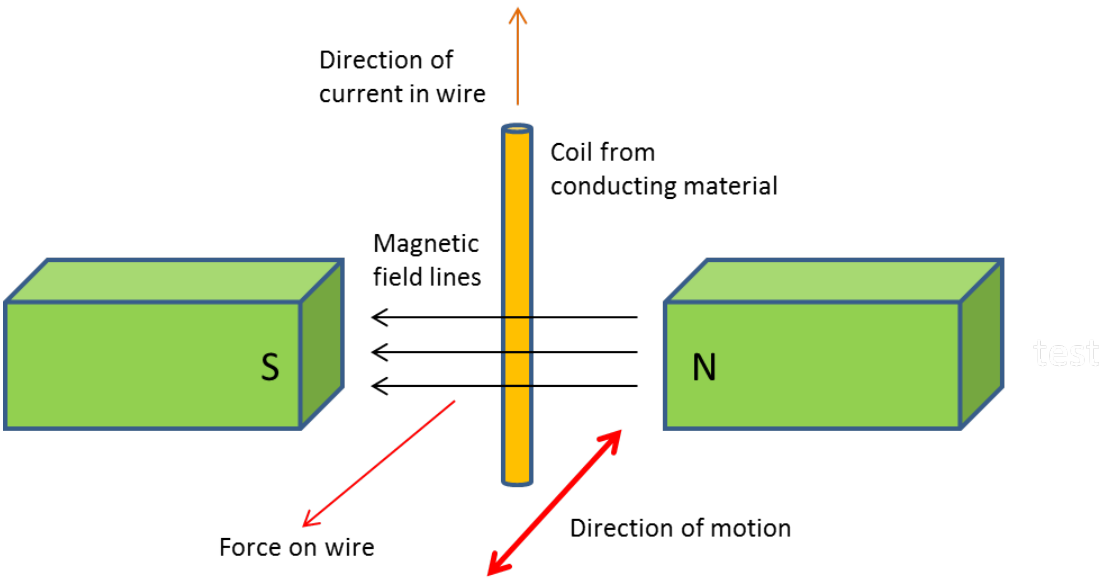

Figure 1.5: Basic principle of electromagnetic induction

1.3 Motion and Kinetic energy

This thesis discusses harvesting of kinetic energy from mechanical vibrations. Environment around us is full of sources of kinetic energy such as the locomotion of living beings, acoustic and audible signals, moving systems and machines and vibrations in nature like earthquakes. Mechanical vibrations are a rich source of kinetic energy as far as quantity and availability. Vibrations are found in bridges, highways, engines, natural geological vibrations, sea waves, and human locomotion, all of these can serve as a source of vibrations and kinetic energy to be harvested.

1.3.1 Mechanical Vibrations

Vibrations are periodic motions of an object [13], such that motion will repeat itself at time interval T. The vibration profile of an object is defined in terms of the amplitude x_o and frequency Ω of the harmonic motion it performs:

$$x(t) = x_o sin(\Omega t) \tag{1.6}$$

where x(t) is the displacement of the object as a function of time t.

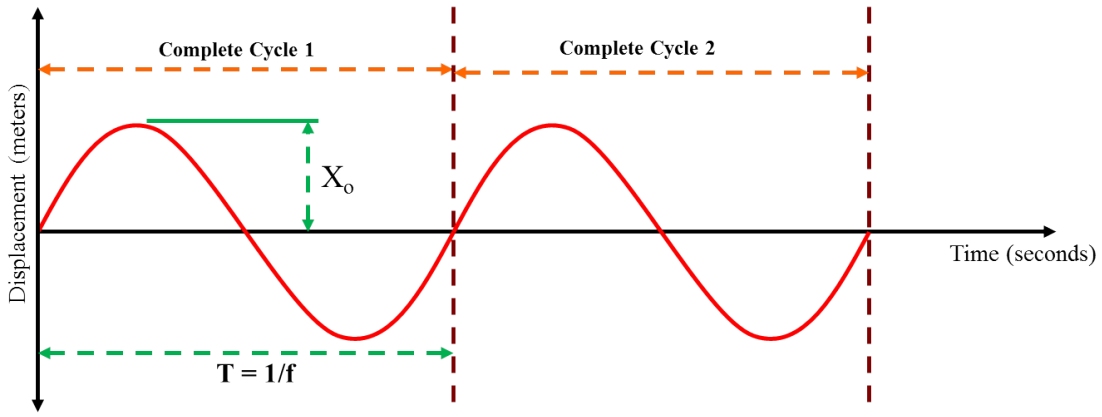

Figure 1.6: An example of Displacement - Time profile of a vibrating body

The time-history of a vibrating body may consist of a fundamental, deterministic tone, or multiple tones, or aperiodic chaotic motion, or stochastic motion. Spectrum analysis can be applied to the time-history of vibrations, such as FFT, to identify the frequency components in the history, the so called "Harmonics".

1.3.1.1 Factors affecting the kinetic energy in vibrations

Three factors affect the kinetic energy in a mechanical oscillator (a vibrating object):

- The mass m of the vibrating body: is proportional to input kinetic energy and therefore should be maximized.
- Stiffness k of the oscillator: defines the center frequency of vibrations.
- Mechanical damping c in the oscillator: defines the fraction of input energy lost.

A schematic of a mechanical oscillator is shown in figure 1.7.

1.3.1.2 Types of Mechanical Vibrations

Vibrations are classified according to:

- Energy source: in to free and forced vibrations.

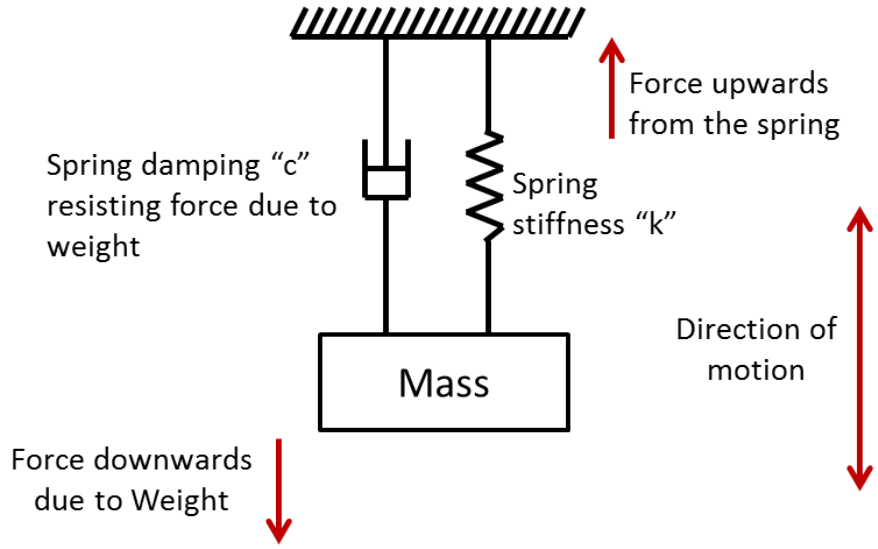

Figure 1.7: A spring-mass-damper oscillator

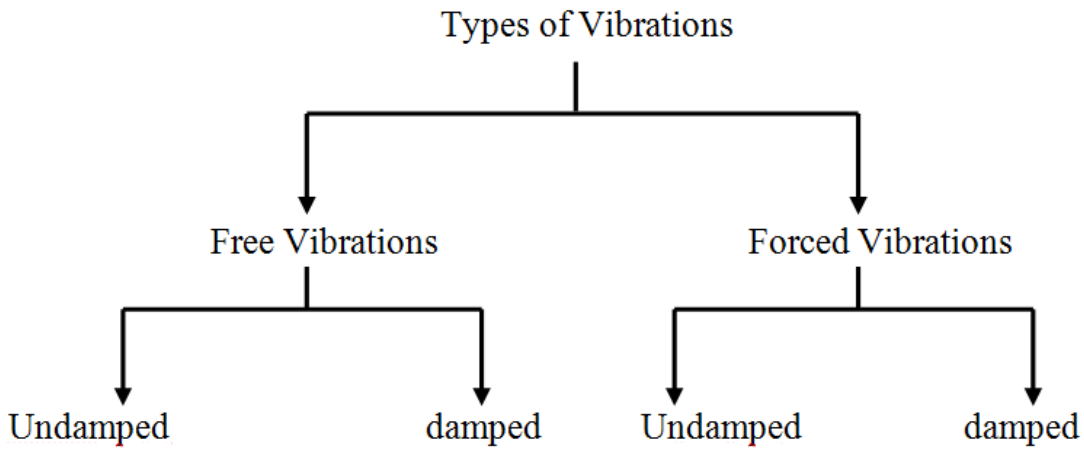

- Energy leakage: into undamped and damped vibrations.

Each of these conditions has its equation of motion and parameters resulting in a different system response, for energy harvesting we are interested in free vibrations either damped or undamped which we are going to discuss.

1. Free - Undamped vibrations Considering the mass and spring shown in figure 1.7 only, the forces acting on this system at equilibrium are the weight and spring force:

$$mg = kx_i \tag{1.7}$$

where x_i is the static equilibrium position. If the mass undergoes free vibrations due to any external disturbance, the mass m will start oscillating up and down away from the static position x_i, according to the equation of motion:

$$-kx = m\ddot{x} \tag{1.8}$$

where x is displacement with respect to the static equilibrium position x_i. The natural frequency ω of this oscillator where the energy level is maximum can be written as:

$$\omega = \sqrt{\frac{k}{m}} \tag{1.9}$$

2. Free - Damped vibrations Practically, damping will exist and due to damping oscillations will decay and die over time. Taking damping into consideration in the equation of motion, results in a n exponential decay in vibration. According to the damping level, we can identify three classes of system response:

   - Over - damped systems: where damping dominates the system response "killing" vibrations and allowing the system to settle down gradually to its equilibrium position.
   - Under - damped systems: where kinetic energy dominates the system response resulting in persistent oscillations as the motion in the system decay and die over long time.
   - Critically-damped systems: where damping and kinetic energy are "balanced" resulting in fast settling down of the system into its equilibrium position.

3. Forced-Damped Vibration In forced vibrations an external force or excitation is applied to the system to force it to vibrate. In the absence of damping, continuous energy supply through forcing leads the system to blow-up if the forcing is high enough to reach the resonance of the oscillator and, therefore, is not of energy interest. On the other hand, in the presence of damping the

oscillator's equation of motion can be written as:

$$m\ddot{x} + c\dot{x} + kx = F_{\circ}\sin(\omega t) \tag{1.10}$$

1.4 Signal Conditioning

The ability of energy harvesters to supply power on demand and in DC form is essential to their successful commercial deployment. On the other hand, the input power from the environment to micro-energy harvesters is intermittent and low. Therefore, an important challenge in the design of micro-energy harvesters is to rectify and store output power in order to guarantee stable, continuous and sufficient supply of power. Further, electromagnetic energy harvesting encounter and additional challenge since its output voltage is on the order of a few to a few hundreds of mili-volts. As a result, three stages of electronic solutions are used to address these challenges:

- Using a charge-pump DC - DC converter, voltage multiplier, or a transformer to boost the output voltage to meet the requirements of electronic power supply and increase the efficiency of rectification circuits.
- Using full-wave or half-wave rectifier bridge circuits to rectify the output of the harvester and stabilize it to a constant level.
- Using a rechargeable battery or a super capacitor to store DC power. The battery or super capacitor will then act as the supply to the target system while the harvester charges the storage element instead of powering the target system directly.

The basic block diagram of an energy harvesting system is shown in figure 1.10.

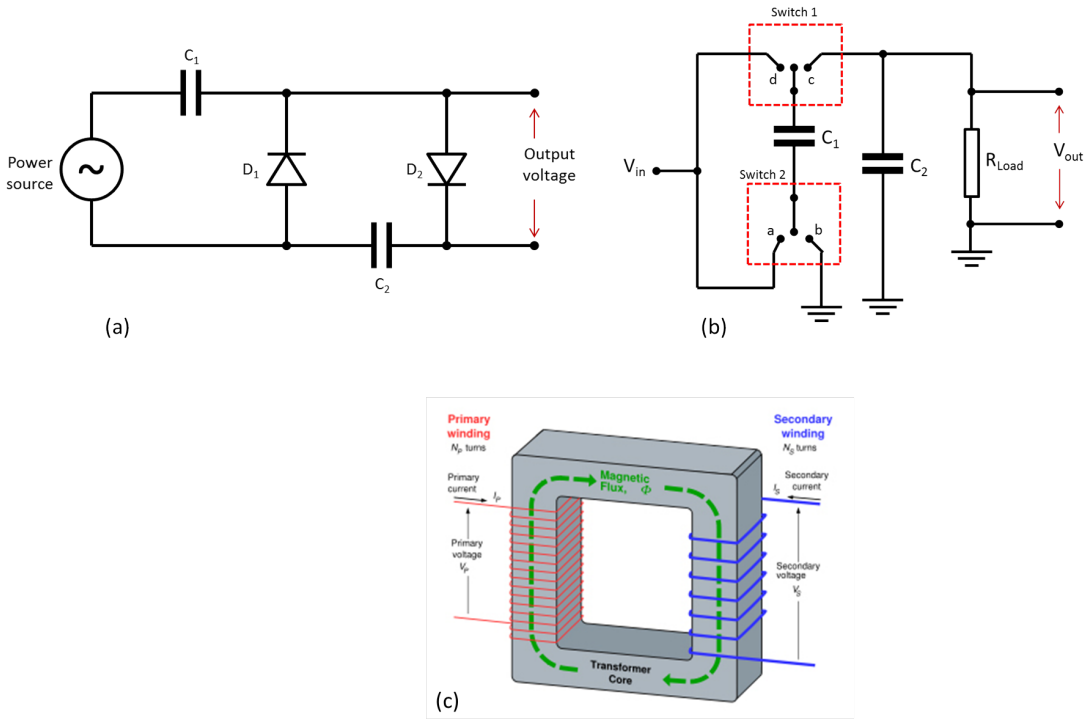

Figure 1.8: (a) Two-stage voltage multiplier, (b) Charge pump DC - DC converter [15], (c) Basic transformer design and winding [16].

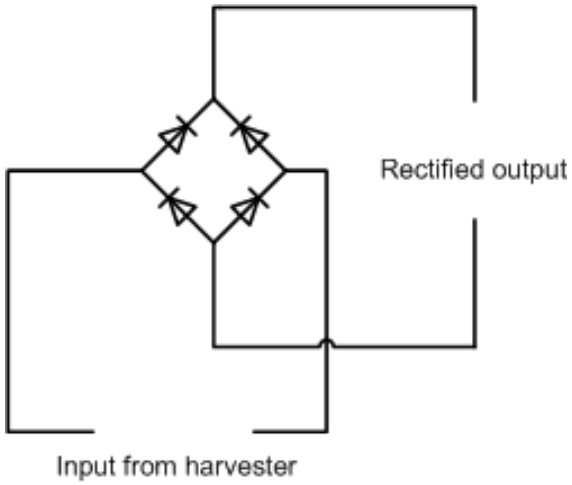

Figure 1.9: Full wave rectifier bridge circuit

1.5 Scope

In this thesis, we study harvesting of environmental vibrations using electromagnetic induction. In particular, we focus on methods and designs that enable the realization of energy harvesters capable of harvesting low-frequency vibrations prevalent

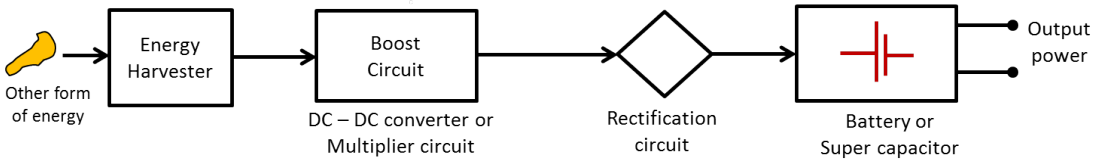

Figure 1.10: Basic design of an Energy harvesting system

in built and naval environments. Towards this goal, two energy harvester designs are introduced in the thesis.

First, we model, analyze, and characterize the springless electromagnetic energy harvester introduced by Mahmoud et. al. We find the system response under various configurations and investigate the nonlinearities appearing in that response.

Second, we introduce a novel electromagnetic energy harvester dubbed the "field disruption energy harvester". The electromagnetic transduction method used here disrupts the magnetic field crossing the coil while the coil and magnets remain stationary. We model, analyze, and characterize this new harvester.

1.6 Thesis Outline

In chapter one, we introduced the technical background and challenges of energy harvesting. We covered the common transduction mechanisms and circuit elements required to provide a stable reliable energy source.

In chapter two, a literature review is conducted on the recent research and trends in energy harvesting. We cover the more common designs used to implement electromagnetic energy harvesters and discuss the advantages and constraints of these designs.

In following three chapters the focus will be on the approach and technologies used to harvest kinetic energy resulted from mechanical vibrations (either artificial or natural vibrations) and converting it to electrical energy through electromagnetic transduction, focusing on two main designs developed by the author and other researchers in the same research group, discussing design parameters , analysis and

results. In the last chapter the author introduces new electromagnetic transduction mechanism for energy harvesting from vibrations, explaining the phenomena behind the mechanism with detailed analysis, model and the mechanical design of a new energy harvester based on this transduction mechanism associated with experimental and lab results and its analysis. System analysis and modeling approaches have been covered in this thesis for the two designs the author designed, tested and verified, studying system dynamics for vibrations based energy harvesting devices and how modifying system dynamics parameters can improve the energy harvested quantitatively and qualitatively, discussing the results and compare it with the recent research approaches and results in this area of science, getting to the conclusion of the research has been conducted by the author in this trend and his recommendations for future work.

Chapter 2

Literature Review

2.1 Introduction

In chapter one, transduction mechanisms used in energy harvesting were discussed. In this chapter, we review literature on energy harvesting from mechanical vibrations with a particular emphasis to electromagnetic energy harvesters. Harvesting energy from vibrations requires an appropriate mechanical design that will interact with the electromagnetic transducer to harvest energy. Two structures are commonly used in energy harvesters:

- Mass - spring - damper
- Beam-supports

Choosing the suitable mechanical structure depends on the environment the harvester will operate in. The type of the structure defines the two central parameters that affect the overall performance of the harvester: its center frequency and bandwidth.

2.2 Mass-Spring-Damper structures

Mass-spring-damper structures are very popular in building vibrations based harvesters because of their simplicity. The model representing this class of harvesters

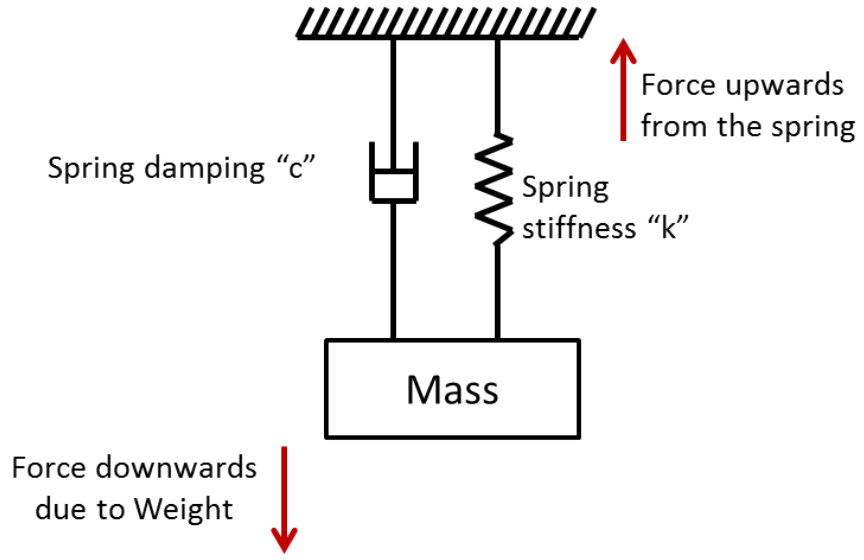

Figure 2.1: Basic mass-spring-damper structure

has been extensively researched and validated. The simplest design in this class is a mass mounted to a vertically aligned spring attached to a source of vibrations as shown in figure 2.1. When external vibrations are applied to the base support of the spring, the mass will move up and down according to the equation of motion:

$$m\ddot{x} + c\dot{x} + kx = -m\ddot{y} \tag{2.1}$$

where x is the relative displacement with respect to the base of the mass from its static equilibrium position.

The center frequency f_o of the harvester depends on the natural frequency of the oscillator:

$$f_o = \frac{1}{2\pi}\sqrt{\frac{k}{m}} \tag{2.2}$$

In figure 2.2, the energy harvester designed by Amirtharajah et al. [4] is shown. It uses a mass-on-spring and electromagnetic transduction to harvest vibrations from human body motion to power medical sensors implanted or placed on the surface of the human body. They achieved a center frequency of $f_o = 94$ Hz and an output power of 400 μW.

Mann et. al. [3] design used a mass-on-spring harvester, figure 2.3, that uses

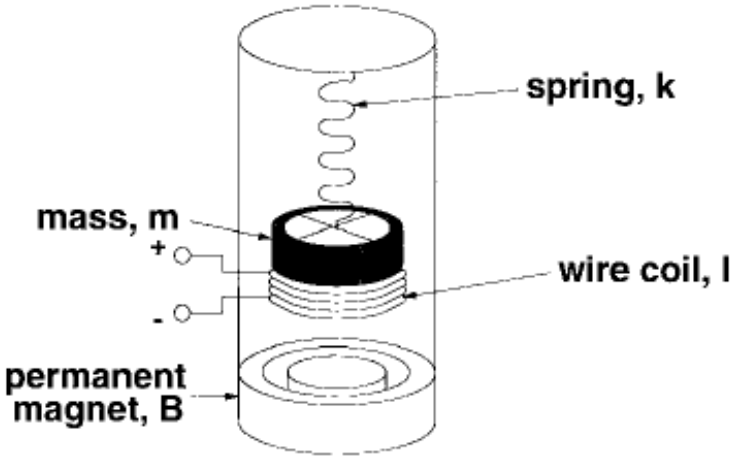

Figure 2.2: Amirtharajah et al. mass on spring based energy harvester design

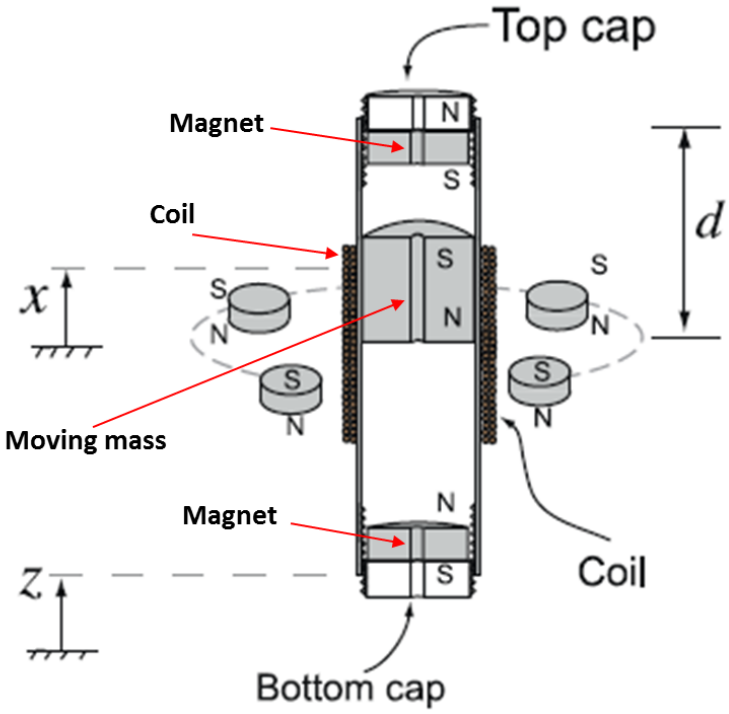

Figure 2.3: Mann et. al. design of mass-on-spring harvester

a magnetic mass and magnets placed at both ends of a tube to serve as springs. Each of the end magnets has a pole identical to that of the magnetic mass facing it. They calculated the center frequency of the harvester as $f_o = 5.12$ Hz and were able to demonstrate an output power up to 200 mW.

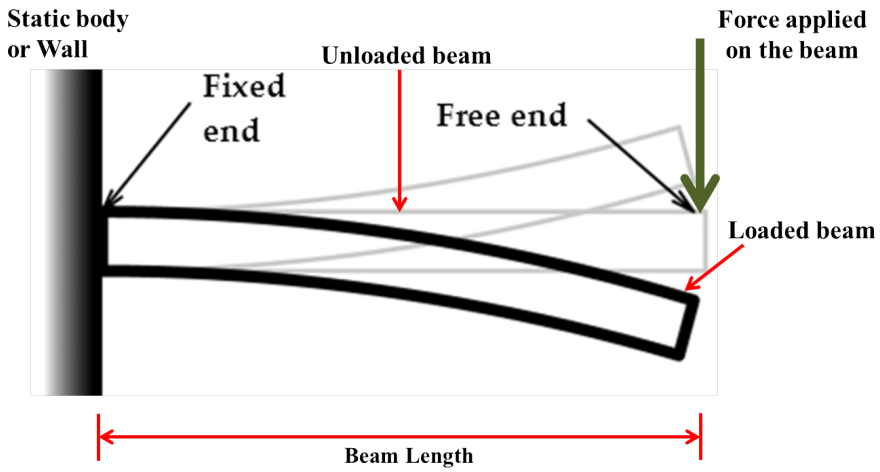

Figure 2.4: Basic Beam - Support structure [17]

2.3 Beam-Support structures

Beam-support structures are the other common class of energy harvesters. Most of these harvesters use either cantilever or guided-end beams to support a seismic mass and/or a coil. The beams in this case behave as springs and add to the seismic mass. Cantilever beam-based, figure 2.2, energy harvesters are widely used. The stiffness of a cantilever beam spring is calculated using the formula

$$k = \frac{3EI}{L^3} \tag{2.3}$$

where E is Young's modulus describing the strength of the material, I is the second moment of area of the beam cross-section, and L is the beam length.

Sari et. al. [6] design used a coil mounted on top of a cantilever beam surface facing magnet poles, figure 2.5, once the cantilever beam is under excitation voltage starts to induce in the coil, achieving center frequency between $3.5 - 4.5KHz$ depending on beam length and maximum output power of $0.4\mu W$

Beeby et. al. [5] design used a coil mounted to the beam free end facing two magnet poles, figure 2.6, achieving center frequency between $52.1 - 53.2KHz$ and maximum output power of $45.8\mu W$

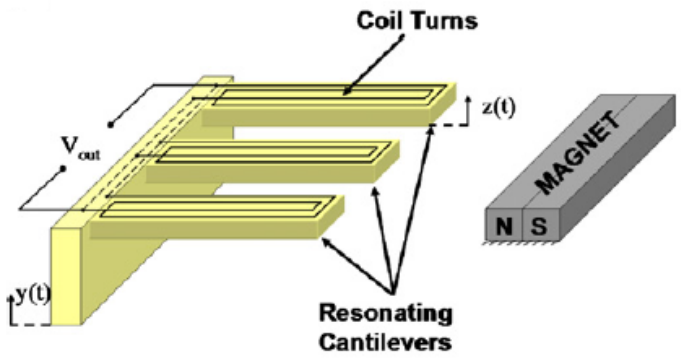

Figure 2.5: Sari et. al. electromagnetic harvester

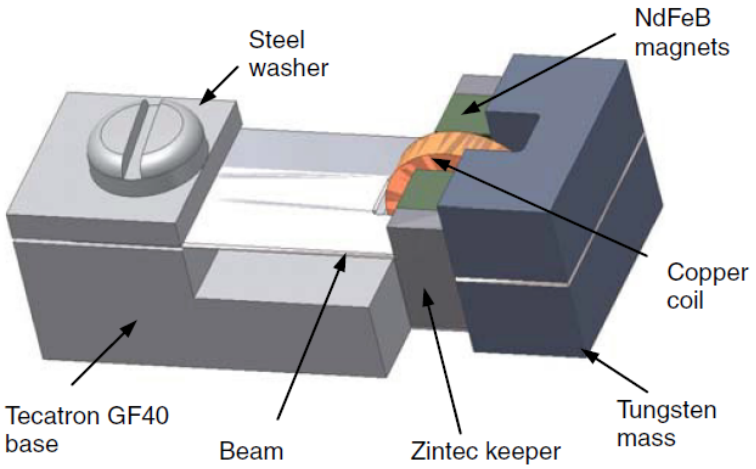

Figure 2.6: Beeby et. al. micro cantilever harvester

2.4 MEMS in energy harvesting

Modern energy harvesters require a small profile for portability and integration into other systems, driving a trend to scale down the mechanical oscillator used in the harvesters. Micro Electro Mechanical Systems (MEMS) technology afforded the tools and mechanisms required to achieve smaller profiles. The past few years has seen intensified work on rebuilding the common structures and models used in vibrations based energy harvesters at micro-scale using MEMS technology. Figure 2.3 a central rigid mass mounted to four crab-leg springs constructed using MEMS technology as a part of an electromagnetic harvester designed by Mostafa et al [9].

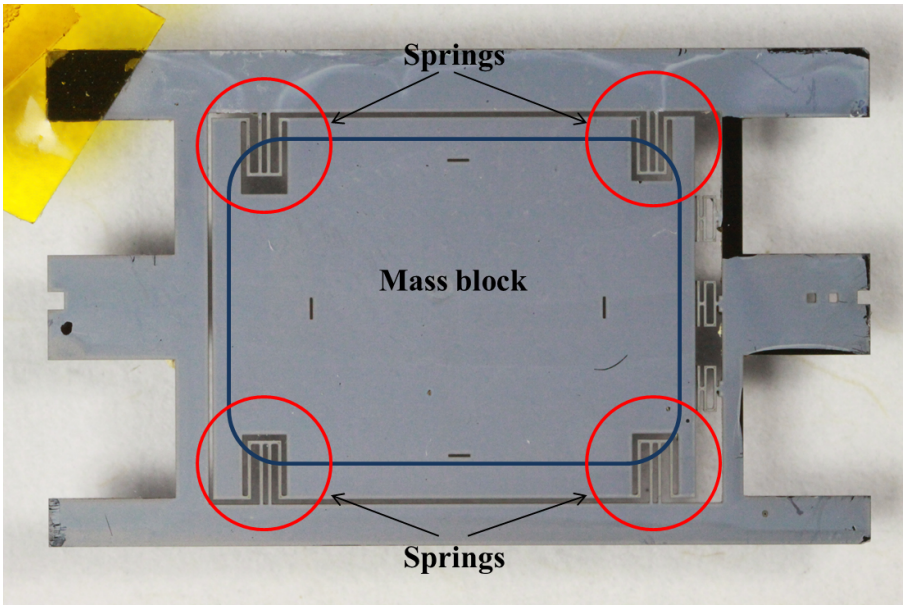

Figure 2.7: Mass mounted to wall with four springs fabricated using MEMS technology

While these types of energy harvesters are capable of generating electrical energy with output power on the order of milli-Watts, their natural frequency must be tuned to match the frequency of ambient vibrations. In environments where ambient vibrations are only available at low frequencies, this proves to be quite a challenge. In many built environments, ambient vibrations are only available at low frequencies. It is therefore impractical to use traditional VEHs that have relatively high center frequency ($\geq$ 10Hz) to harvest low frequency ($\leq$ 10Hz) vibrations. As a result, there has been an interest in realizing low center frequency VEHs.

Wang et. al. [7] used mass-on-spring structure to design an electromagnetic based harvester at MEMS scale, mounted an inertial magnet mass mounted on spiral net-like spring and below the mass-spring structure a stationary coil mounted on the device base, harvesting with the oscillation of the spring, figure 2.8, achieving center frequencies around 48.58 and 146.72 Hz and able to output up to 104 nW.

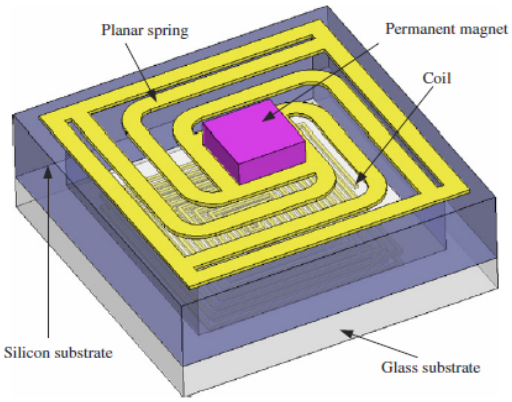

Figure 2.8: Mass mounted to wall with four springs fabricated using MEMS technology

2.5 Power flow

Maximizing the output power is a major concern when designing energy harvester, where three factors affect the output power level:

- Mechanical losses.
- Damping in the system (electrical and mechanical).
- Natural frequency.
- Load impedance.

Mechanical losses, damping and natural frequency are handled through various mechanical design techniques, where matching the electric output impedance of the harvester with the load impedance and tuning the harvester natural frequency to the vibrations harvested are the efficient and commonly used methods to maximize output power.

Assuming a linear oscillator [10] excited by a base acceleration $A\cos\Omega t$, the peak velocity of the seismic mass m occurs when the frequency of excitation Ω matches the natural frequency of the harvesting oscillator ω. It can be written as

$$v_p(t) = \frac{m}{c} A \sin(\omega t + \phi) \tag{2.4}$$

where Q is the quality factor of the harvester. The average velocity over one cycle of oscillations at peak conditions is

$$v_{Avg} = \frac{m}{c}\frac{A}{\sqrt{2}} \tag{2.5}$$

where c is the total damping coefficient of the harvester. Therefore, the average input kinetic energy per cycle is

$$E_{Avg} = \frac{1}{2}mv_{Avg}^2 = \frac{m^3A^2}{4c^2} \tag{2.6}$$

and the average input power at peak conditions is

$$P_{in} = E_{Avg}f_\circ = \frac{m^3}{c^2}\frac{A^2}{4}f_\circ \tag{2.7}$$

where $f_\circ = \frac{2\pi}{\omega}$ is the center frequency of the harvester.

While equation (2.7) indicates that increasing the size of the seismic mass will increase the input power, it will also change the mechanical damping of the harvester. Therefore, we must determine the optimal inertial mass analytically by taking the derivative of the input power with respect to mass. Since the damping c and center frequency $f_\circ$ are functions of mass, we substitute for them and take the derivative with respect to m to obtain

$$\frac{A^2m\sqrt{km}}{4\pi c^2}(\frac{5}{4} - \frac{m}{c}\frac{\partial c}{\partial m}) = 0 \tag{2.8}$$

In order to estimate the damping c as a function of the mass m, the other system parameters are held constant, while a series of discrete mass sizes are used to estimate the damping coefficient. The experimental setup used consisted of a closed-loop electromagnetic shaker used as source of base excitations.

$$Q = \frac{f_\circ}{\Delta f}$$

The damping coefficient was, then, found using the relationship

$$c = \frac{\omega m}{Q}$$

Chapter 3

Horizontally Aligned Springless Energy Harvester

3.1 Introduction

In this chapter we model, analyze, and test the springless electromagnetic vibrations-based energy harvester (VEH). The performance of this VEH depends on its alignment with respect to the gravitational potential field. In this chapter, we address the VEH when it is align perpendicular to gravity. We dub this configuration the horizontally-align springless VEH.

The VEH [8] of interest is shown in Figures 3.1 and 3.2. It represents a single-degree-of-freedom oscillator following the discrete mass structure. The electromagnetic transducer is made of a cage containing permanent magnets, which serves also as the inertial mass, moving along a linear guide with respect to a stationary coil printed on a PCB. The inertial mass moves freely along the linear guide except at the ends where two springs act as end limiters. As the mass moves along the linear guide, the magnetic field lines crossing the coil lines, the magnetic field lines are being cut by the stationary coil causing an induced potential difference to develop cross the coil inducing a potential difference between the coil terminals.

The oscillator attains maximum velocity, and thus input kinetic energy, in a

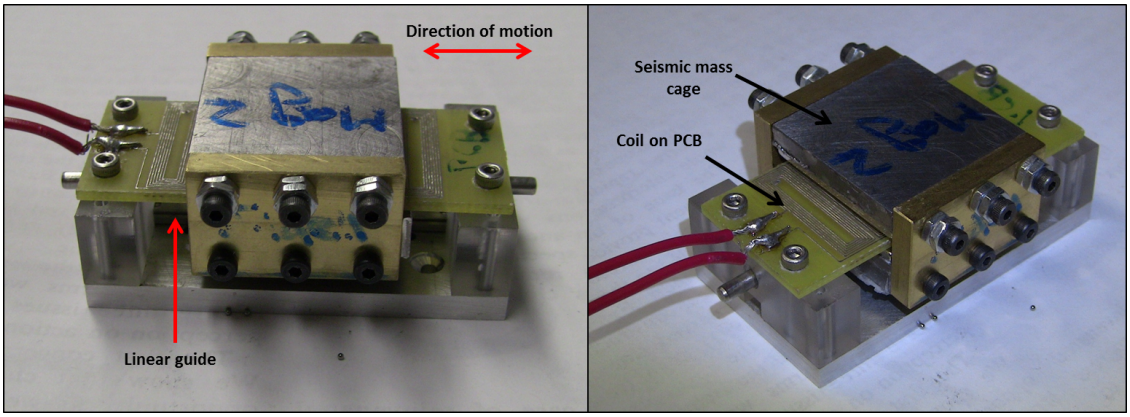

Figure 3.1: Electromagnetic Vibrations based Energy Harvester

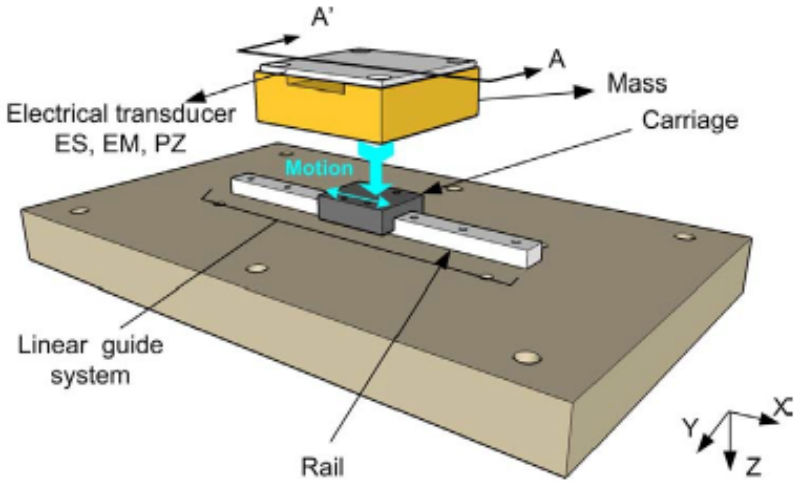

Figure 3.2: VEH design

frequency band around its natural frequency defined as:

$$f_o = \frac{1}{2\pi}\sqrt{\frac{k_{eff}}{m}} \tag{3.1}$$

where k_{eff} is the effective stiffness of the oscillator due to the intermittent contact between the mass and the end springs. The fact that the inertial mass is supported by a linear guide rather than a spring and sees spring forces only while in contact with the end limiters reduces the effective stiffness of the oscillator and allow us to target low-frequency vibrations.

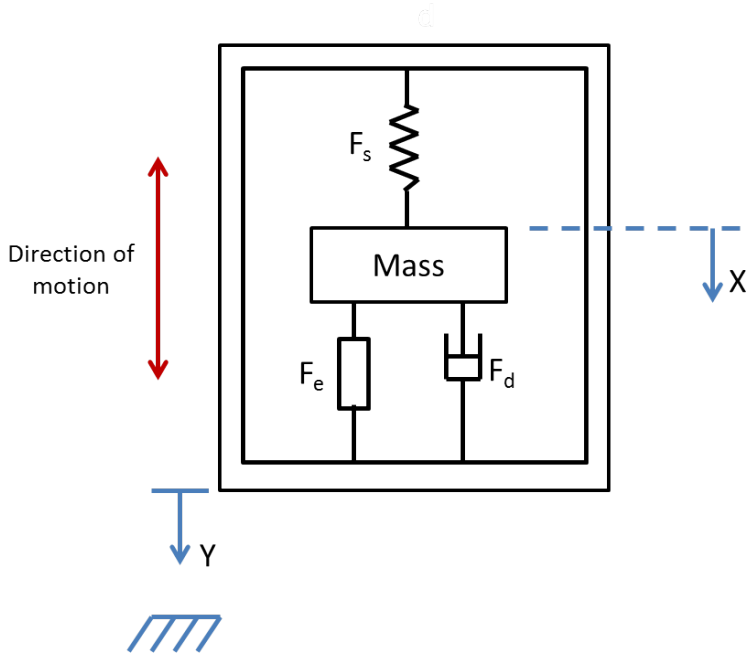

Figure 3.3: Mass-Spring-Damper based VEH design

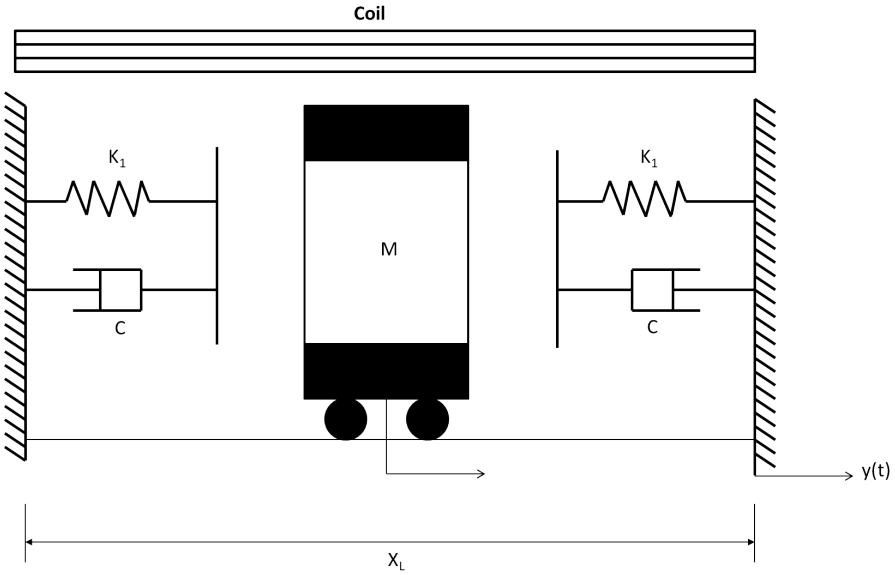

Figure 3.4: Schematic of the horizontally aligned springless VEH

3.2 Modeling springless VEH

The springless VEH consists of an electromagnetic transducer, an inertial mass comprised of magnets and a cage, and a carriage running freely along a linear guide. The carriage moves along the linear guide carrying the assembly with respect to a

stationary surface coil in response to base excitations, as shown in Figure 3.4. The motion of the carriage induces a voltage V across the coil terminals and proportional to the time rate of change of the magnetic flux within the coil

$$V = -\frac{d\phi}{dt}\frac{dx}{dt} \tag{3.2}$$

where ϕ the total magnetic flux and x is is the displacement of the magnetic field with respect to the coil.

The horizontal implementation of the VEH, Figure 3.4, is suitable for environments where motions are predominantly in the horizontal direction. The linear guide, aligned horizontally, allows the carriage to move along the rail while baring motion in other directions. The carriage carries the inertial mass and the transducer along the guide. The equation of motion of the horizontally-aligned harvester is:

$$m\ddot{x} = -(b_e + b_m)\dot{x} - F(x) - m\ddot{y} \tag{3.3}$$

where x and y are the displacements of the seismic mass m and frame, respectively, and F(x) is the restoring force. The VEH harvests kinetic energy transmitted to it from the host vibrations represented by the base acceleration:

$$\ddot{y} = Acos(\Omega t) \tag{3.4}$$

where A and Ω are the amplitude and frequency of the external excitation. Two identical springs are used as limiters on either end of the linear guide. The origin of the coordinate system is placed at equal distance from the two end limiters (midpoint of the linear guide). The seismic mass m is assumed to be a point mass, as shown in Figure 3.5.

The restoring force F(x) varies with the position of the inertial mass m as it

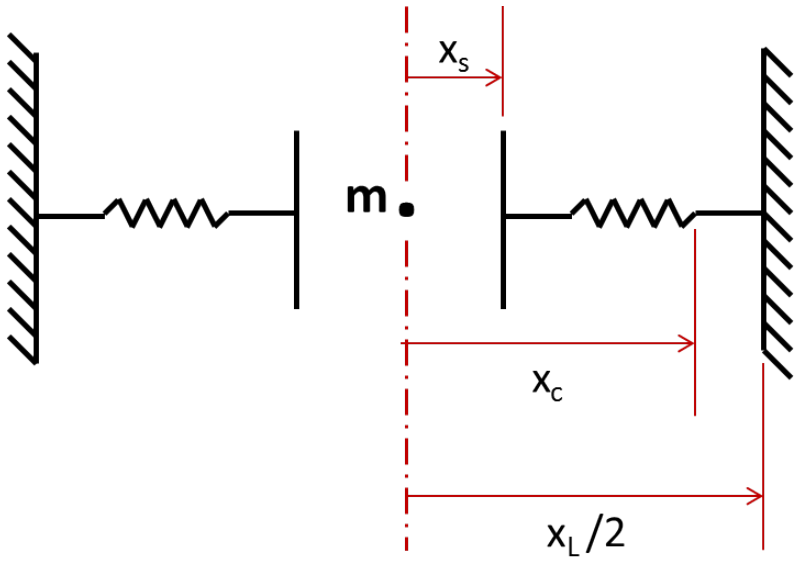

Figure 3.5: Lumped-mass model of the horizontally aligned springless VEH

moves between the two end limiters according to the equation:

$$F(x) = \begin{cases} 0 & |x| \leq x_s \\ k_1(x - x_s) & x_s \leq |x| \leq x_c \\ k_1(x - x_s) + k_2(x - x_c) + \alpha(x - x_c)^3 & x_c \leq |x| \leq \frac{x_L}{2} \end{cases} \tag{3.5}$$

where x_s is the position where the mass touches the free (uncompressed) spring, x_c is the position where the spring is fully compressed, x_L is the length of the linear guide, k_1 is the linear spring stiffness, k_2 the linear stiffness of the fully compressed spring, and α is the coefficient of cubic nonlinearity of the fully compressed spring. The force-displacement relationship is shown in Figure 3.6.

3.3 Electromagnetic Damping

The current passing through the coil creates a magnetic field that opposes the field produced by the magnets. The interaction between the two fields produces a force which opposes the motions of the inertial mass. This interaction force is the

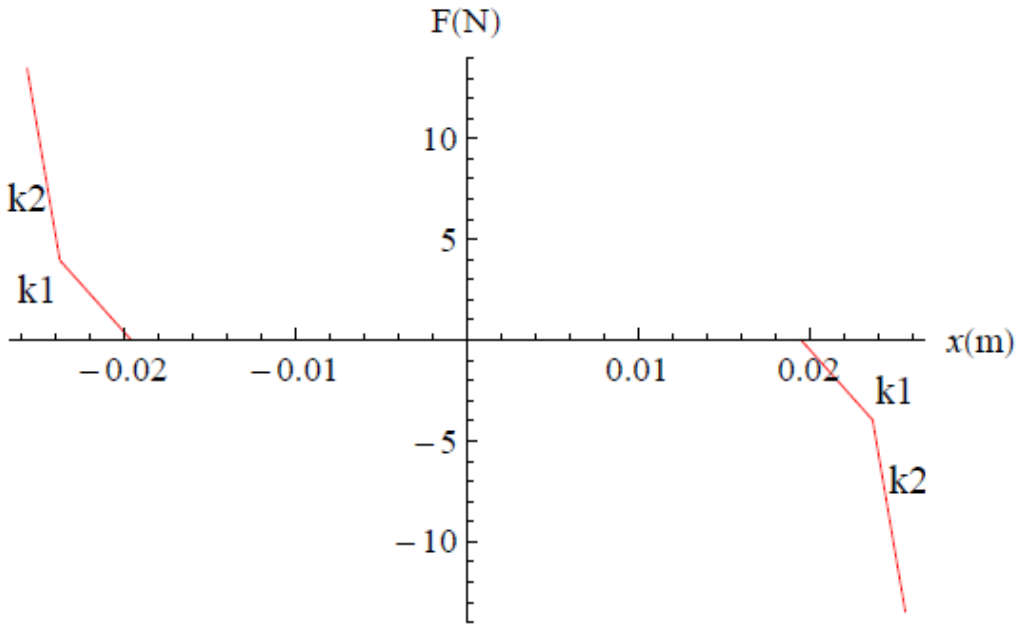

Figure 3.6: The end springs force-displacement relationship

electromagnetic damping defined as:

$$F_{em} = b_e \dot{x}, \tag{3.6}$$

The electrical power extracted from the mechanical oscillator is given by:

$$P_{em} = F_{em} \dot{x} = b_e \dot{x}^2, \tag{3.7}$$

This power is dissipated in the parasitic coil resistance RC and the load resistance R_L. Equating the power dissipated in the coil and load to that extracted from the oscillator gives:

$$b_e \dot{x}^2 = \frac{V^2}{R_L + R_C + j\omega L}, \tag{3.8}$$

Where L is the coil inductance. Substituting Equation 2.1 into Equation 2.7 we

obtain the electromagnetic damping b_e as:

$$b_e = \frac{1}{R_L + R_C + j\omega L}\left(\frac{d\phi}{dx}\right)^2, \tag{3.9}$$

Since the coil inductance is negligible and assuming that the coil moves in a region of constant magnetic field, the electromagnetic damping coefficient can be expressed as:

$$b_e = \frac{(N\,B\,l)^2}{R_L + R_C}, \tag{3.10}$$

Where B is the magnetic field intensity, N the number of turns and l is the effective length of the coil. The electrical damping for the prototype under test can be calculated using Equation (2.9) and the parameter values in Table 2.1.

Table 3.1: Electromagnetic Transducer Parameters

Parameter	Value
Magnetic Field: B (T)	0.37
Effective Coil Length: l (m)	1.74
Load Resistance: R_L (Ω)	8.2
Coil Resistance: R_C (Ω)	4.4

3.4 Mechanical Damping

The frequency-response curve of the open-loop harvester is used to determine the mechanical quality factor Q_m of the VEH from the formula

$$Q_m = \frac{f_\circ}{\Delta f}, \tag{3.11}$$

where $f_\circ$ is the center frequency and $\Delta f = f_2 - f_1$, with f_1 and f_2 the two half-power frequencies. The mechanical damping coefficient is then found as

$$b_m = \frac{\sqrt{m\,k}}{Q_m}, \tag{3.12}$$

We can find the mechanical damping b_m using Equations 2.11 and 2.10 and the values of the systems parameters given in Table 2 as $b_m = 0.411kg/s$. The center frequency and half power bandwidth were found from a frequency sweep of the base acceleration of the VEH at an amplitude of $A_o = 0.1$ g. The total damping of the VEH is sum of mechanical damping and electromagnetic damping: $b = b_e + b_m$.

Table 3.2: VEH Parameters

Parameter	Value
Mass: m (Kg)	0.095
Stiffness: k_1 (N/m)	950
Center Frequency: $f_\circ$ (Hz)	14.091
Lower $3dB$ Frequency: f_1 (Hz)	13.784
Upper $3dB$ Frequency: f_2 (Hz)	14.394

3.5 Experimental Results

A prototype of the designed VEH was mounted on an electromagnetic shaker, Figure 3.7, where the experimental setup schematic is shown in figure 3.8, and a base acceleration was applied as input excitation. The RMS of the open-loop voltage between the coil terminals was measured using a data acquisition system. The VEH was tested by applying an input base excitation.

$$\ddot{y} = A_\circ \cos \Omega t \tag{3.13}$$

Where A_o and ω are the amplitude and frequency of the excitation. The frequency of the base acceleration was swept up and down the frequency range 3 to 12 Hz while the amplitude was held constant at 0.1, 0.2, 0.3 and 0.4g.

Figure 3.9 shows the frequency-response curves of the RMS output voltage. As the excitation amplitude increases, the frequency-response curves bend further to the right indicating the existence and increase in the level of a hardening-type non-linearity. We also note the existence of jumps in the frequency-response curves between co-existing upper and lower response branches. As the frequency is slowly

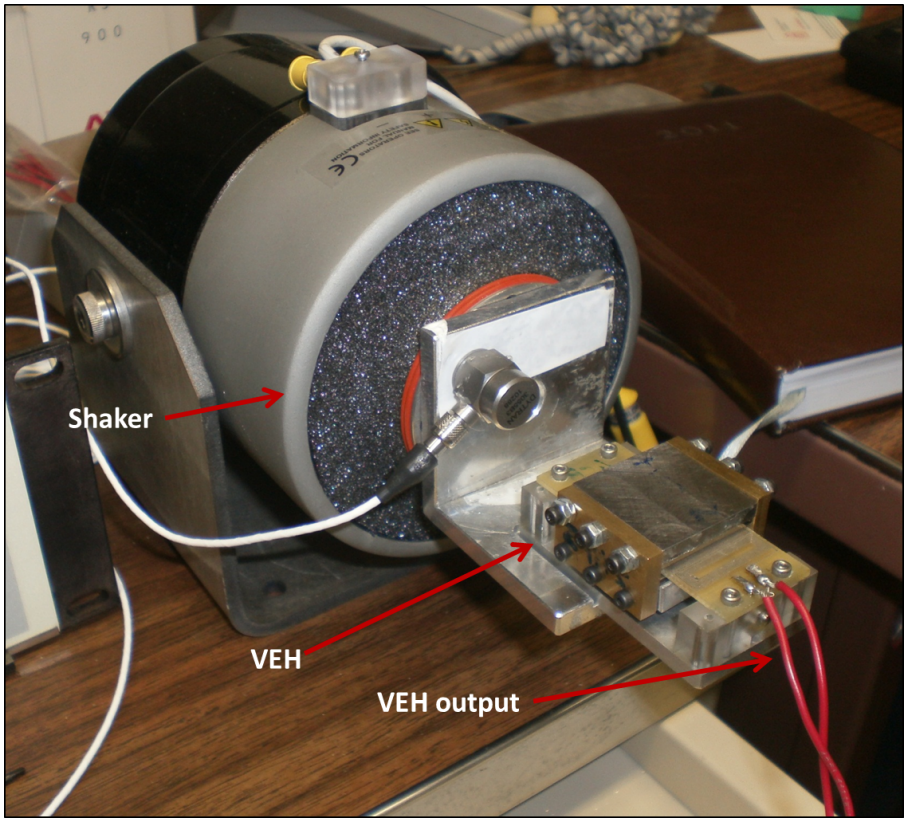

Figure 3.7: Experimental Setup of the VEH

increased, the response curve reaches a peak along the upper branch before suddenly dropping onto the lower branch. As the frequency is then decreased, the system follows the lower response branch further into the left of the first jump location before jumping back to the upper response branch. The difference between the locations of the jump-down and jump-up indicates the size of the region of multivaluedness and, therefore, the strength of the nonlinearity in the system. We note that the hysteretic region expands as the excitation amplitude increases indicating that the level of the hardening effective is increasing. Table 3.3 lists the peak amplitude and frequency of the frequency-response curves as well as the size of the region of multivaluedness (hysteretic region).

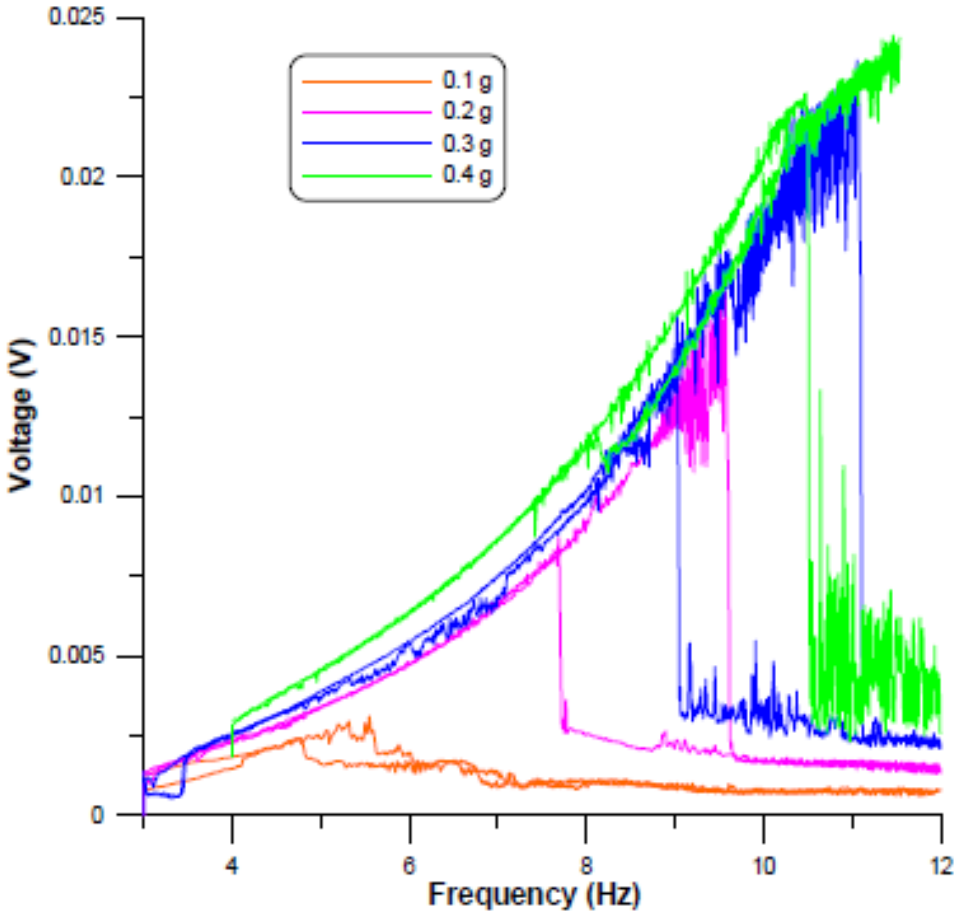

Figure 3.8: Experiment Setup Schematic

Table 3.3: Nonlinear resonance amplitude and frequency for base acceleration amplitudes of $A_\circ = 0.1, 0.2, 0.3$, and $0.4\,\mathrm{g}$

Acceleration Amplitude (g)	Peak Amplitude (V)	Frequency (Hz)
0.1	0.0025	5.5
0.2	0.0175	9.8
0.3	0.0225	10.6
0.4	0.024	11.2

3.6 Model Results

The model, Equation 3.2, was used to obtain the displacement of the seismic mass and open-loop voltage of the coil. Substituting Equation 3.4 into the ordinary differential equation 3.2 and integrating numerically for base acceleration amplitude

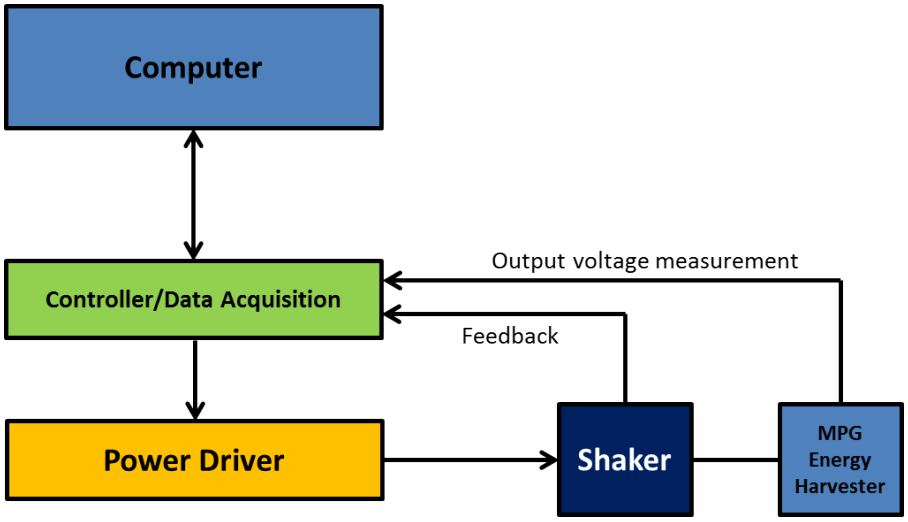

Figure 3.9: The frequency-response of the coil RMS voltage for base acceleration amplitudes of $A_o = 0.1, 0.2, 0.3$ and $0.4g$

of A = 0.4g and frequency of $\Omega = 14Hz$, we obtain the time-history of the displacement of the seismic mass and the open-loop voltage in the coil shown in Figures **??** and 3.11 respectively. The results indicate that the seismic mass engages the two end springs but does not fully compress them, which is consistent with the experimental observations for this excitation level, and the harvested voltage is approximately 25mv. The output peak-to-peak voltage from the harvester recorded with an oscilloscope, Figure 3.13, shows that the output waveforms from the harvester and generated from the model are the same but with difference in amplitude, indicating that the model results model are qualitatively correct and reflects the harvester response.

A spectral analysis via FFT, Figure 3.12 of the model response shows peaks at the forcing frequency as well as higher harmonics with significant peaks at 2Ω and 3Ω indicating the presence of quadratic and cubic nonlinearities. The quadratic nonlinearity appears due to the damping effects of the electromagnetic force acting on the seismic mass.

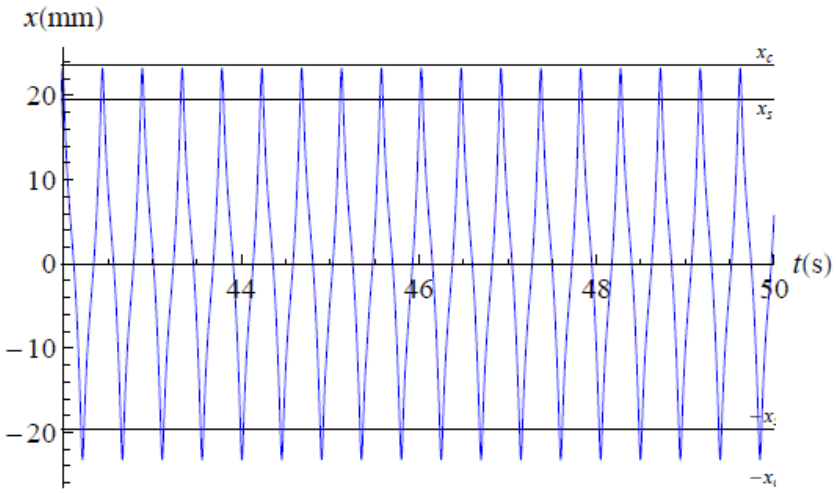

Figure 3.10: Seismic mass displacement for an excitation of amplitude $A_o = 0.4g$

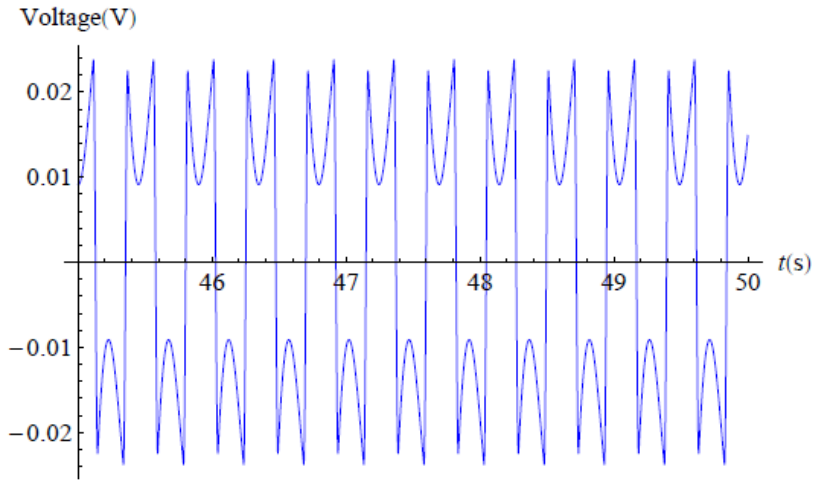

Figure 3.11: Seismic mass displacement for an excitation of amplitude $A_o = 0.4g$ (*voltage* vs *Time*)

3.7 Summary

In this chapter a design of a vibrations based energy harvester introduced, discussing the theory of operation, modeled and analyzed the response of a horizontally-aligned low-frequency springless vibration energy harvester. We tested the VEH experimentally and found that its response depends on the amplitude and frequency of base excitations. We also observed that as the base excitation was varied form 0.1 g to 0.4 g and the frequency was swept from 3 to 12 Hz, a consistent bending

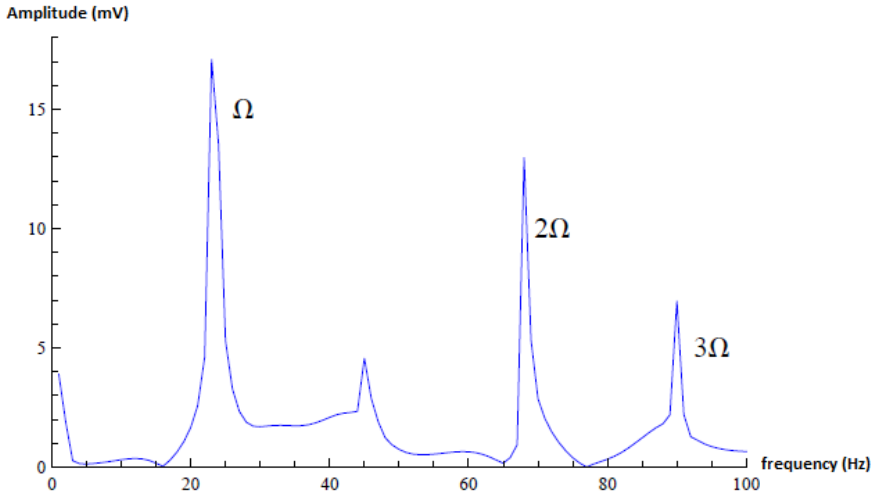

Figure 3.12: Spectral analysis via FFT for the model response

Figure 3.13: Output peak-to-peak voltage waveform from the harvester captured on oscilloscope

of the frequency response curves of the coil RMS voltage to the right indicating an effective hardening-type nonlinearity. The FFT spectrum of the seismic mass displacement shows the presence of both quadratic and cubic nonlinearities in the system response. The hardening cubic nonlinearity appears due to the end limiters configuration, while the dominant quadratic nonlinearity is driven by the electro-

magnetic coupling of the transducer (magnets and coil) to the impact oscillator motions.

Chapter 4

Vertically Aligned Vibrations Based Energy Harvester

4.1 Introduction

In this chapter we will examine the same springless VEH discussed in the previous chapter but under the influence of vertical oscillations to harvest energy [11], the results monitored showed a significant difference in the system response and system behavior than the system behavior of the same springless VEH under horizontal oscillations. The harvester is positioned so that its oscillations are aligned vertically acting against gravity. The MPG response is investigated experimentally. Test results show that the VEH behaves as a softening nonlinear oscillator even for small excitations. A mathematical model of the underlying impact oscillator is also derived and its parameters are estimated.

4.2 Mathematical Model

The springless VEH consists of an electromagnetic transducer, an inertial mass comprised of magnets and a cage, and a carriage running freely along along a linear guide. The carriage moves along the linear guide carrying the assembly with respect to a stationary surface coil in response to base excitations, as shown in figure 3.1.

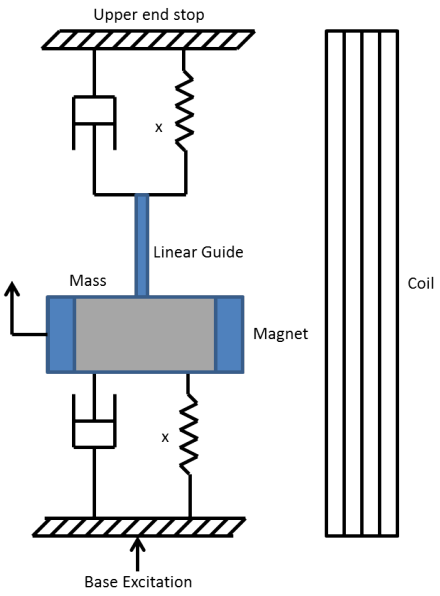

Figure 4.1: Vertical Implementation of the VEH

The vertical implementation of the VEH, Figure 4.1, is suitable for environments where motions are predominantly in the vertical direction. The linear guide in this case is aligned with the direction of gravity. It allows the carriage to move along the rail while baring motion in other directions.

The carriage carries the inertial mass and the transducer along the guide. The equation of motion of a vertically-aligned harvester is:

$$m\ddot{x} + (b_e + b_m)\dot{x} + F(x) = -m\ddot{y} - mg \tag{4.1}$$

where x and y are the displacements of the seismic mass m and frame, respectively. The origin of the coordinate system used to describe the seismic mass is placed at the position where it just touches the uncompressed lower spring. The seismic mass m is assumed to be a point mass, Figure 4.2. The free distance along the rail (not occupied by the cage) between the upper and lower uncompressed springs is denoted x_t. The uncompressed length of each spring is denoted x_s and the fully compressed length is denoted x_c.

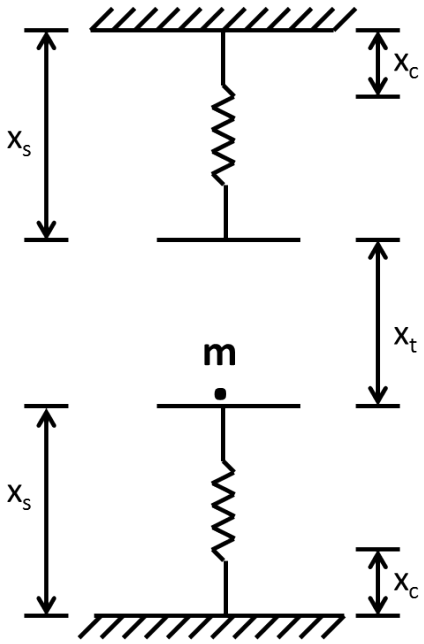

Figure 4.2: Simplified Schematic of the VEH

The restoring force is represented by a piecewise nonlinear spring as follows:

$$F(x) = \begin{cases} k_2(x + x_s - x_c) & -x_s \leq x < x_c - x_s \\ \quad +k_1(x_c - x_s) + \alpha x^3 & \\ k_1 x + \alpha x^3 & x_c - x_s \leq x < 0 \\ 0 & 0 \leq x < x_t \\ k_1(x - x_t) + \alpha(x - x_t)^3 & x_t \leq x < x_t + x_s - x_c \\ k_2(x - x_t - x_s + x_c) & x_t + x_s - x_c \leq x \\ \quad +k_1(x_s - x_c) + \alpha(x - x_t)^3 & \quad < x_t + x_s \end{cases} \tag{4.2}$$

where k_1 is the linear spring stiffness, $k_2 \gg k_1$ is the stiffness of the fully compressed spring, and α is the spring coefficient of cubic nonlinearity. The force-displacement relationship is shown in Figure 4.3.

Three distinct motion regimes can be identified for the vertically-aligned VEH:

- For small excitations (motions where $x_c - x_s < x \leq 0$): the seismic mass will be in contact with the lower spring throughout motion and the system will behave as a nonlinear oscillator with a linear stiffness k_1 and a cubic

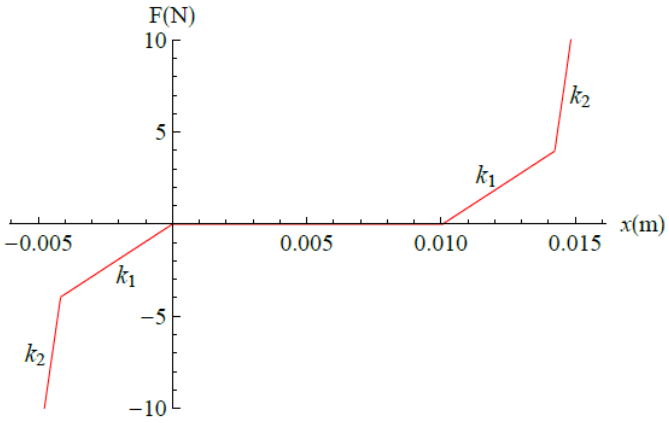

Figure 4.3: force-displacement relationship of the spring

hardening nonlinearity α.

- For moderate excitations (motions where $x < x_t$): The amplitude of oscillation will be large enough for the seismic mass m to separate from the lower spring without reaching the upper spring.

- For large excitations (motions where $-x_s \leq x \leq x_s + x_t$): Motions will be large enough for the seismic mass to leave the lower spring, fly freely along the rail, contact the upper spring, before descending again.

4.2.1 Damping

The electrical damping can, therefore, be calculated using Equation 3.9 and the parameter values given in Table 3.1.

We can find the mechanical damping using Equation 3.12 and the values of the systems parameters given in Table 4.1 as $b_m = 0.411kg/s$. The center frequency and half power bandwidth were found from a frequency-sweep of the base acceleration of the VEH at an amplitude of $A_o = 0.1g$. The total damping of the VEH is sum of mechanical damping and electromagnetic damping: $b = b_e + b_m$.

Table 4.1: VEH Parameters

Parameter	Value
Mass m (kg)	0.095
Stiffness k_1 (N/m)	950
Center Frequency f_0 (Hz)	14.091
Upper $3dB$ Frequency f_2 (Hz)	14.394
Lower $3dB$ Frequency f_1 (Hz)	13.784

4.3 Results

A prototype of the proposed VEH was mounted on an electromagnetic shaker and a base acceleration was applied as input excitation. The RMS of the open-loop voltage between the coil terminals was measured using a data acquisition system. The VEH was tested by applying a frequency-sweep of Ω in the domain of interest while holding the amplitude of base acceleration constant A_o.

4.3.1 Small Excitations ($A_o \leq 0.1g$)

Figure 4.4 shows the experimentally obtained frequency response curves of the RMS voltage for up- and down-sweeps of the base acceleration at amplitudes of $A_o = 0.1g$ (red), 0.05g (blue), 0.025g (green), and 0.02g (blue). The up-sweeps are shown in solid lines and the down-sweeps in dashed lines. The data were oversampled and then decimated at the rate of 1-to-10 using Matlab function Decimate. The VEH exhibits a softening effective nonlinearity as indicated by the curves bending to the left and the nonlinear resonance peak shifting to lower frequencies as the excitation amplitude increases; even for the very lowest levels of excitation. This fact indicates the harvesting oscillator should be treated as a nonlinear oscillator even for small excitations. Model output, Figure 4.5, shows a similar waveform for small excitations to the actual output with difference in amplitude level, indicating that the model results are qualitatively consistent with the experimental results.

The model, Equation (4.2), was used to obtain the displacement of the seismic mass and open-loop voltage of the coil for base acceleration amplitude $A_o = 0.1g$ and center frequency = 14.2 Hz. After the transient response, the system settles

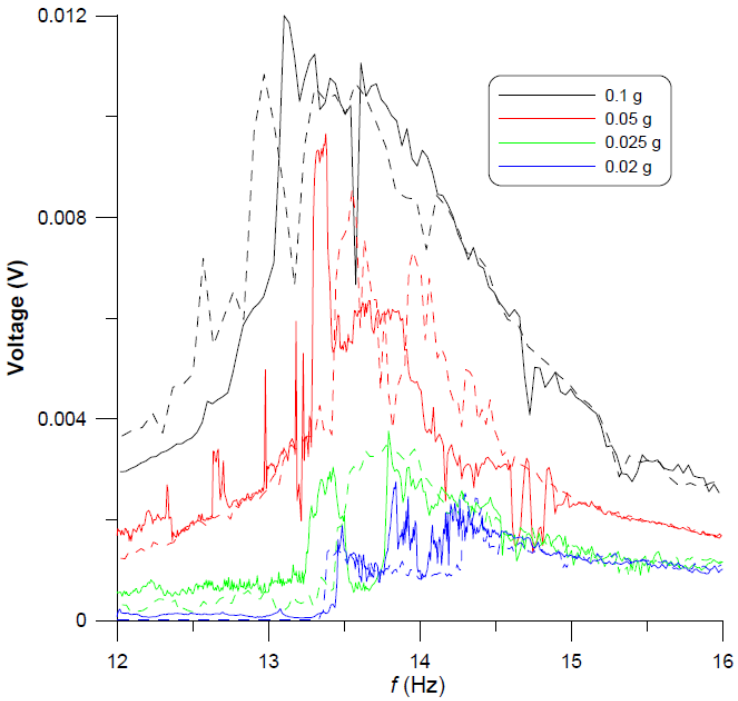

Figure 4.4: The frequency-response of the coil RMS voltage under low excitations

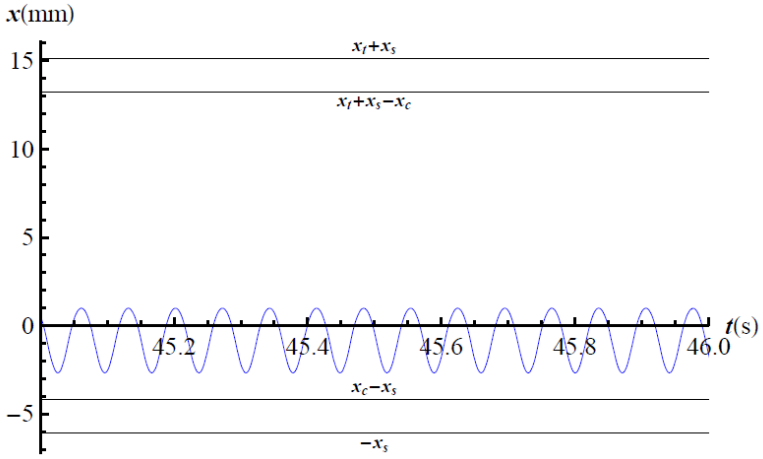

Figure 4.5: Time-history of the seismic mass displacement $x(t)$

down to the steady-state response shown is Figure 3.5. We observe that the oscillations are just starting to separate from the spring for a short interval during the cycle.

An FFT, Figure 4.6 of the model response shows peaks at the forcing frequency Ω as well as higher harmonics with significant peaks at 2Ω and 3Ω indicating the

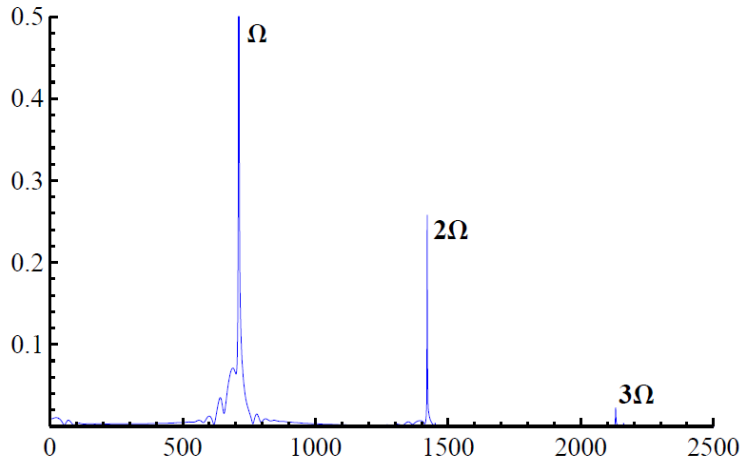

Figure 4.6: FFT of the seismic mass displacement at $A_o = 0.1g$

presence of quadratic and cubic nonlinearities. The quadratic nonlinearity appears due to the damping effects of the electromagnetic force acting on the seismic mass.

4.3.2 Moderate Excitations ($0.1g < A_o < 0.2g$)

For base acceleration amplitudes greater than 0.1g and less 0.2g, the seismic mass separates from the lower spring to travel along the linear guide without touching the upper spring. The experimental frequency-response curve of the coil RMS voltage is shown in Figure 4.7 for an intermediate acceleration amplitude of $A_o = 0.15g$. The figure presents an up-sweep (red line) and a down-sweep (blue line) of the excitation frequency in the interval [10 - 18] Hz. Clear evidence emerges in the results for the coexistence of two branches (upper and lower) of response, jumps between these branches, and hysteresis in the VEH response. During the up-sweep, a jump occurs from the lower response branch to the upper branch at 12.6 Hz, whereas a jump occurs during the down-sweep from the upper branch to the lower branch at 12.2 Hz.

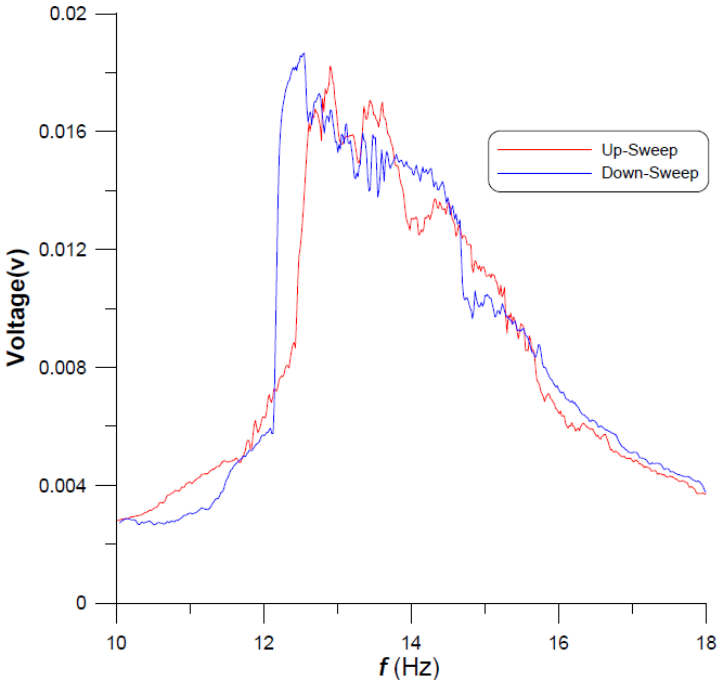

Figure 4.7: Frequency-response of the coil RMS voltage for an acceleration amplitude of $A_o = 0.15g$

4.3.3 Large Excitations ($A_o > 0.2g$)

The base acceleration amplitudes were set to $A_o = 0.2$ g, 0.3 g, and 0.4 g to test the VEH response to large excitations (motion regime 3). Up- and down-sweeps of the frequency of excitation were performed in the interval 10 Hz to 18 Hz and the RMS of the voltage across the coil was measured experimentally. The resulting frequency-response curves are shown in Figure 4.8 in solid lines for the frequency up-sweeps and dashed lines for the frequency down-sweeps. Consistent with the previous test cases, all frequency response curves are bent to the left indicating softening type nonlinearity. As in the case of moderate excitations, jumps between an upper and a lower branches of response and hysteresis between the up- and down-sweeps are observed. The hysteretic region in the frequency spectrum grows to cover more than 1 Hz and shifts to lower values along the frequency spectrum as the acceleration amplitude grows. Specifically, the region of multivaluedness shifts down from [11.5 - 13.3] Hz at $A_o = 0.2g$ to [10.6 - 11.9] Hz at $A_o = 0.4g$.

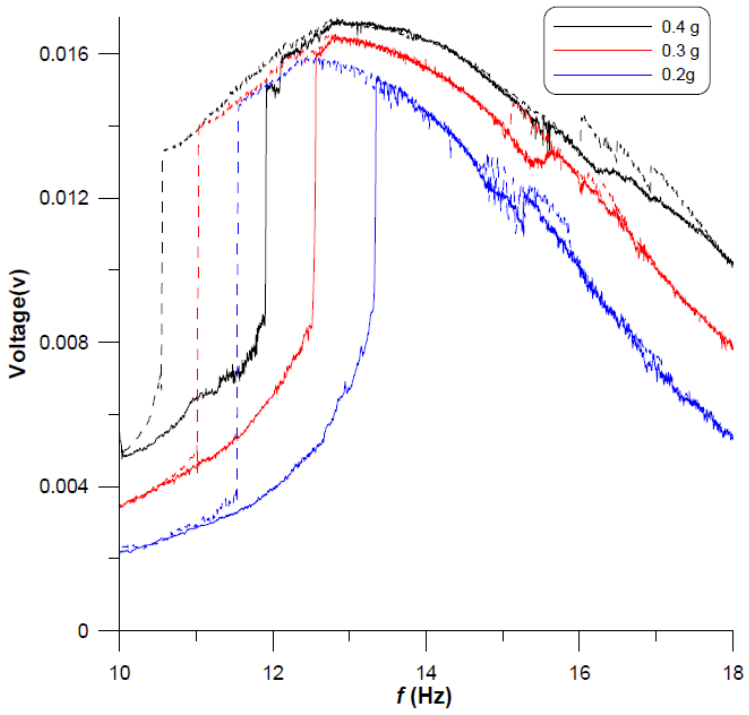

Figure 4.8: The frequency-response of the coil RMS voltage under large excitations

Additional features are also observed in the VEH response within this motion regime. The peak voltage is effectively capped to approximately 16mV at 12.4 Hz for $A_o = 0.2g$, 12.8 Hz for $A_o = 0.3g$, and 12.7 Hz for $A_o = 0.4g$. These peaks appear because the mass oscillations are interrupted as they grow when the flying mass impacts the upper spring. As a result, the seismic mass displacement saturates as it covers most of the available range of motion between the upper and lower springs. During a down-sweep from the peak, the amplitudes of the velocity and coil voltage drop linearly since the displacement amplitude remains almost stationary as the frequency drops, which creates the negative-slope lines segments to the left of the peaks. Eventually, and once the frequency is far enough from resonance, the response falls back to the lower branch during a down-sweep or decrease in size, during an up-sweep, to cease impacting the upper spring and follow the normal upper response branch of a softening-type frequency-response curve. This process has the dual effects of capping the realizable output voltage and expanding the energy harvesting (half-power) bandwidth of the VEH. This is

quite advantages since it allows us to realize a wider energy harvesting bandwidth at a lower point along the frequency spectrum.

4.4 Summary

In this chapter we modeled and analyzed the response of a vertically-aligned low-frequency springless vibration energy harvester. We tested the VEH experimentally and found that its response contains three distinct regions of operation depending on the amplitude and frequency of base excitations. In all three regions, we observed a consistent bending of the frequency response curves of the coil RMS voltage to the left indicating an effective softening-type nonlinearity. The FFT spectrum of the seismic mass displacement shows the presence of both quadratic and cubic nonlinearities in the system response. The hardening cubic nonlinearity appears due to the end limiters configuration, while the dominant quadratic nonlinearity is driven by the electromagnetic coupling of the transducer (magnets and coil) to the impact oscillator motions. Further, the spring-type end-limiters were found to saturate the realizable output voltage to a maximum proportional to the track length but allow for a much wider energy harvesting bandwidth as the base excitations amplitude increases.

Chapter 5

Field Disruption Energy Harvester

5.1 Introduction

In this chapter, a novel electromagnetic transduction mechanism is introduced to generate electricity from harvested kinetic energy. The transduction mechanism, dubbed "Induction by Field Disruption", is based on placing a coil winding between two (or more) sources of magnetic field with opposite polarity and allowing a ferromagnetic object to cut the magnetic field lines, thereby disrupting the magnetic field cutting the coil and resulting in an induced potential difference across the coil terminals. The assembly is attached to a host body where waste motions or vibrations are available. Host motions cause the free moving ferromagnetic object to travel along a track cutting the magnetic field lines. The high permeability ferromagnetic material of the object increases the concentration of field lines in the vicinity of the position of the object. This disruption in magnetic flux induces an electric potential V between the coil terminals. The track, for example a low-friction dielectric tube, ferromagnetic object, and end limiters placed at the ends of the track comprise a mechanical oscillator. While the harvester can produce electric energy from any of the ferromagnetic object motions, it is particularly useful in harvesting electric energy out of host oscillations that have a frequency close to

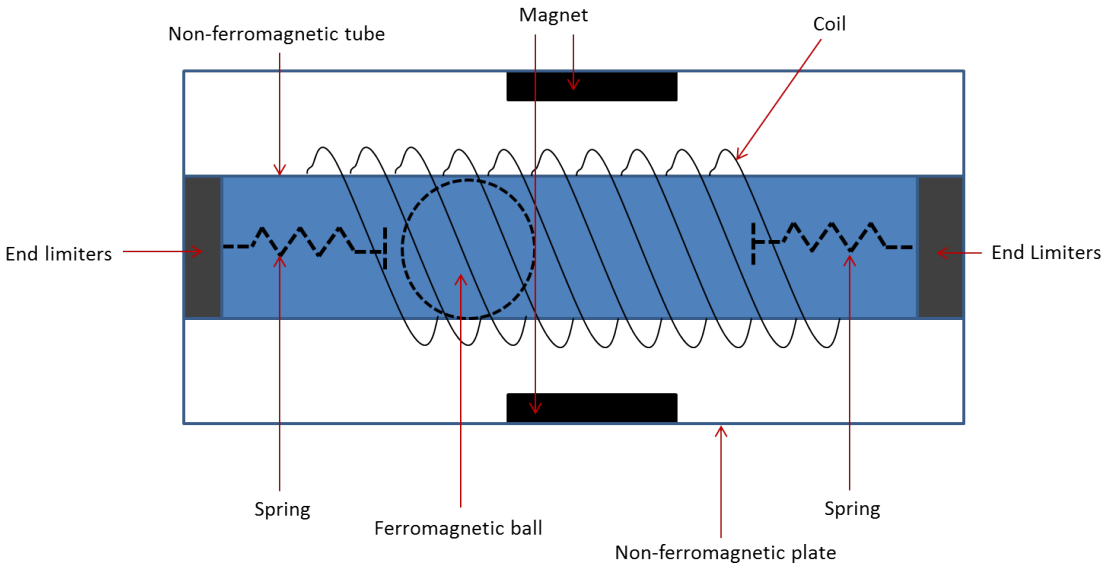

Figure 5.1: Two-dimensional harvester

the natural frequency of the mechanical oscillator.

5.2 Harvester Concept

The Field Disruption Harvester (FDH) consists of an electromagnetic transducer, a coil wound around a tube and number of magnets surrounding the coil-tube assembly, and an inertial mass moving freely along the tube.

A conducting coil is wound around a tube, preferably made of non-ferromagnetic material. Inside the tube, a free moving object, preferably a ferromagnetic ball, moves along a low-friction track, such as a smooth tube, a lubricated track, or a linear guide. Two end-limiters are mounted to the tube ends to terminate the object motions, preferably made of low-loss springs. A number of magnets (one or more) are mounted outside the tube to create a magnetic field within the tube. The tube and magnets are mounted to a plate, in a two-dimensional version, or a container, in a three-dimensional version to maintain their relative positions. The plate or the container is preferably made of a non-ferromagnetic material to maintain maximum field intensity within the tube. The carrier plate or container is rigidly mounted to a host that supplies kinetic energy (waste motions or vibrations).

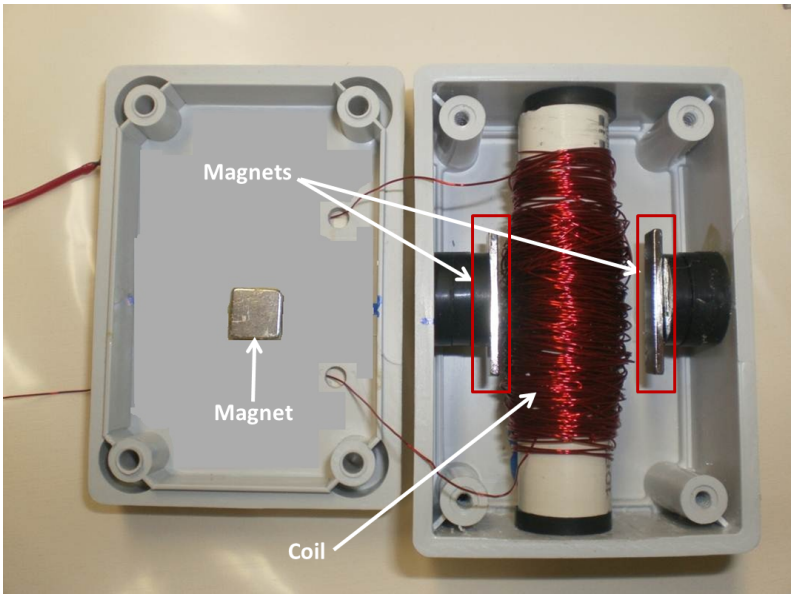

Figure 5.2: A picture of the three-dimensional FDH

A schematic of a two-dimensional FDH is shown in Figure 5.1. A conducting coil mounted to a plastic tube is placed on a non-ferromagnetic plate. Magnets are mounted on the plate above and below the tube. Two springs mounted to the end caps of the tube are used as end-limiter on either end of the tube. A steel ball moved freely inside the tube.

5.2.1 Three-Dimensional FDH

In the three-dimensional version of the harvester, copper wire is wound around a plastic tube and a steel ball (ferromagnetic object) is placed inside it. The assembly is places inside a plastic box (non-ferromagnetic container). Four magnets are mounted to the box and placed in close proximity of the tube; specifically they are placed on both side and at top and the bottom of the tube. A picture of a prototype for a three-dimensional FDH is shown in Figures 5.2.

A schematic top view of the FDH is shown in Figure 5.3. The drawing illustrates the placement of the steel ball and the two end limiters. The end-limiters are made of steel helical springs backed by rubber desks mounted directly to the walls of the container. Figure 5.4 shows a front-view of the three-dimensional harvester. The

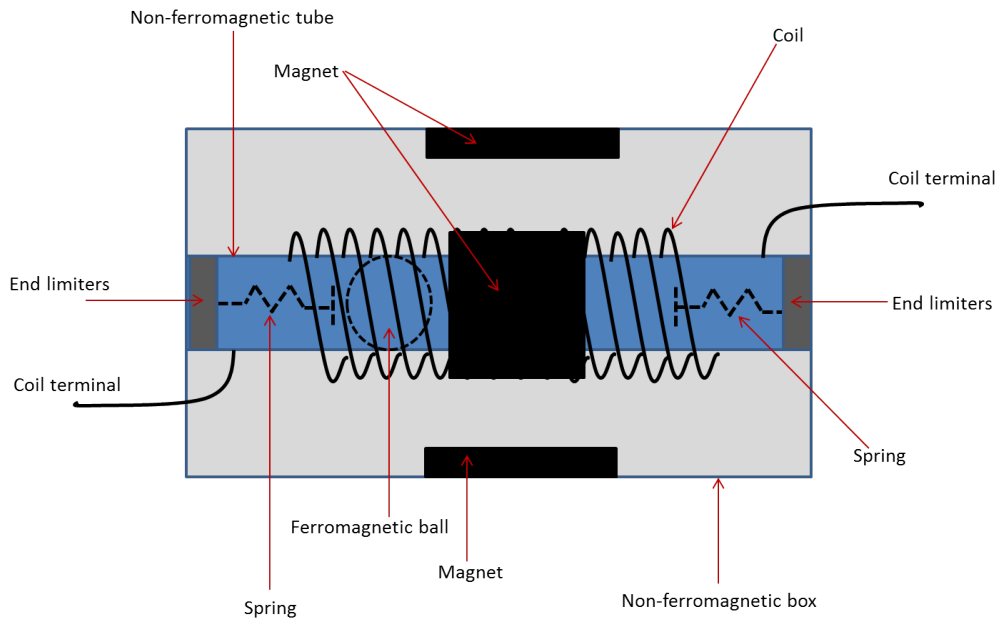

Figure 5.3: Top-view of the three-dimensional FDH

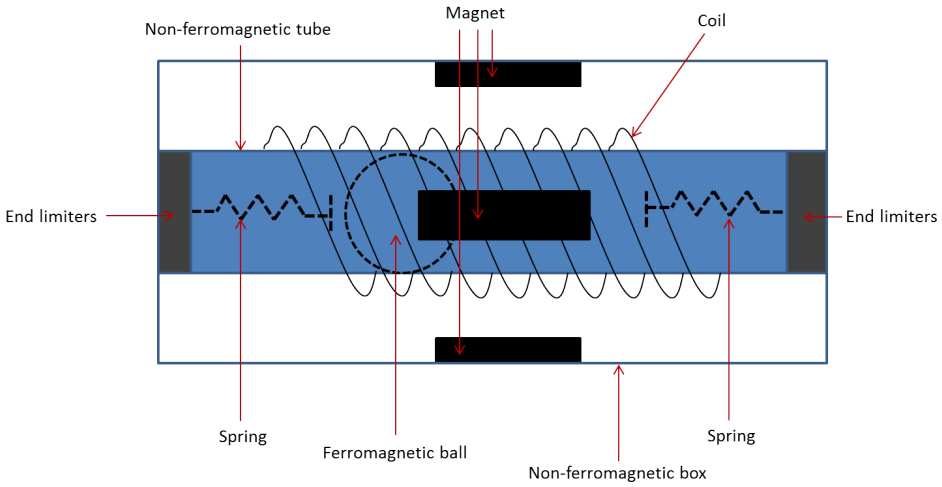

Figure 5.4: Front-view of the three-dimensional FDH

drawing illustrates the placement of the magnets above, below, and beside the tube.

Figure 5.5 shows a side-view of the three-dimensional harvester. The drawing illustrates the placement of the four magnets above, below, and on both sides of the tube. It also shows the concentric placement of the coil, tube, and ball as well as the concentric placement of the tube, rubber desks, and helical springs. Figure 5.6 shows a cross-section of the FDH at a position along the tube axis where the

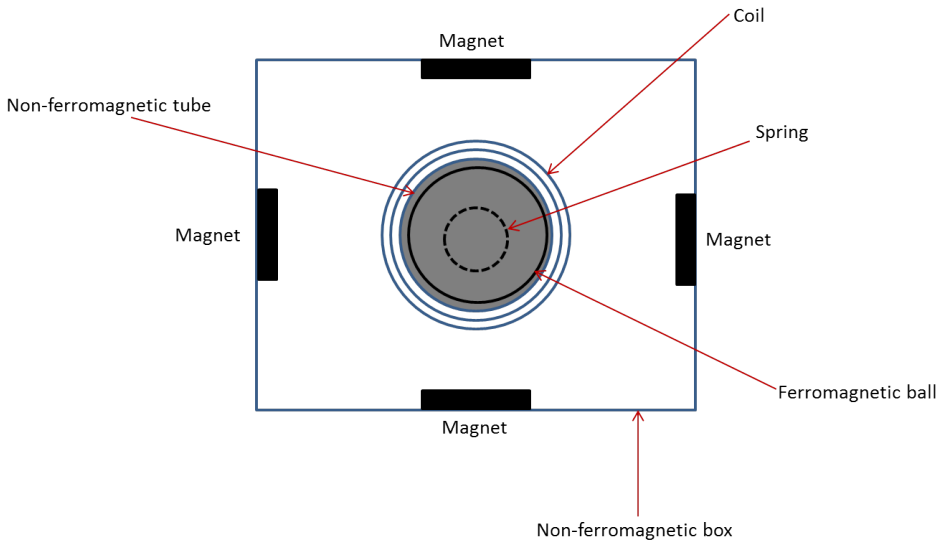

Figure 5.5: Side-view of the three-dimensional FDH

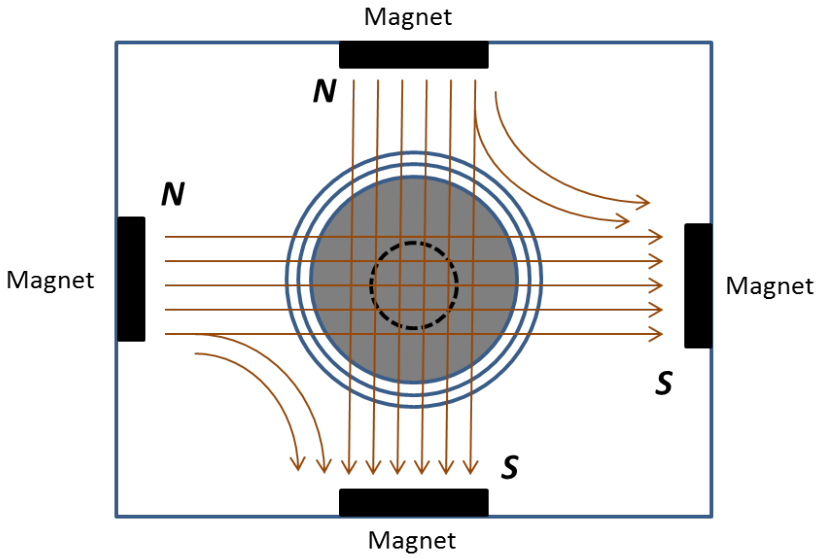

Figure 5.6: A cross section of the FDH at an axial position adjacent to the magnetic field sources

magnetic field sources are adjacent to the tube. The figure shows the placement of the magnets around the dielectric tube and the magnetic flux in the vicinity of the tube. Each of the horizontal and vertical pairs of magnets are arranged such that the facing poles have opposite polarity. The distance between the horizontal pair of magnets and the surface of the plastic tube d_1 and d_2 and the vertical pair of magnets d_3 and d_4 in the fabricated FDH prototype are listed in Table 5.1. The

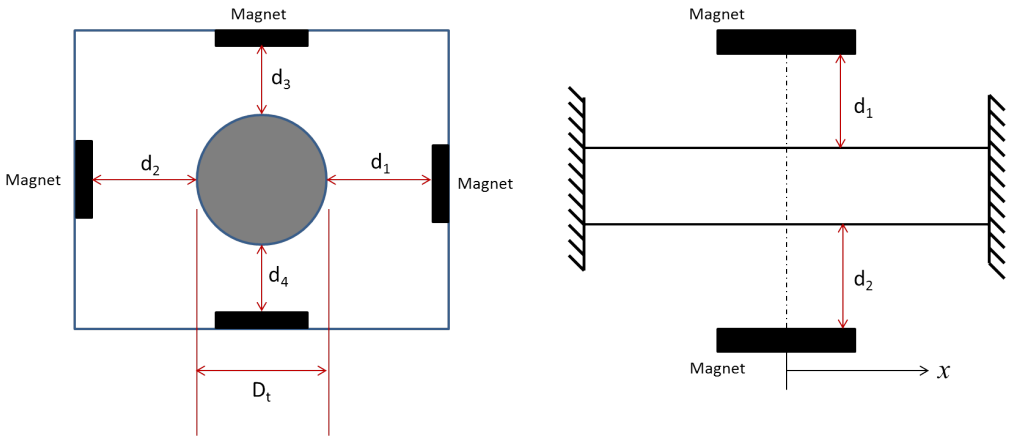

Figure 5.7: FDH Dimensions

table also lists the measured coil resistance R_c and the magnitude of the magnetic field intensity at the center of the tube $B_\circ$ in the absence of the ball.

Table 5.1: Magnetic field Parameters

Parameter	Value
Distance between side magnets and track: d_1, d_2 (mm)	5.6
Distance between upper/lower magnets and track: d_3, d_4 (mm)	13.59
Track outer diameter: D_t (mm)	15
Coil resistance: R_c (Ω)	5.4
Magnetic field intensity: $B_\circ$ (mT)	28

5.3 Harvester Model

The steel ball moves freely along the tube in response to base excitations $y(t)$ of the tube. The motion of the ball $x(t)$ relative to the tube induces a voltage $V(t)$ across the coil terminals. The equation of motion of the ball describes the balance between the absolute acceleration of the ball the $(\ddot{x} + \ddot{y})$ and the forces applied to it:

$$m(\ddot{x} + \ddot{y}) = c_m\dot{x} + c_e\dot{x} - F_s(x) - F_m(x) \tag{5.1}$$

where m is the ball mass, $c_m\dot{x}$ is the mechanical damping force acting on the ball, $c_e\dot{x}$ is the electromagnetic damping force applied by the coil to the ball, and $F_s(x)$

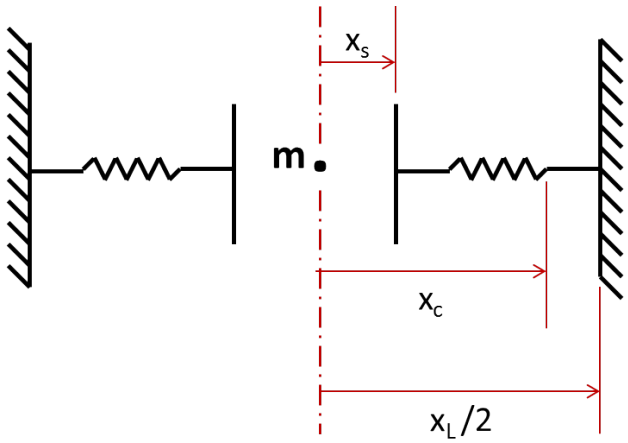

Figure 5.8: A schematic of an oscillator representing the FDH

and $F_m(x)$ are the mechanical and magnetic restoring forces acting on the ball, respectively.

Table 5.2: Track Parameters

Parameter	Value
Track length: x_t (mm)	72
Unstretched spring length: x_s (mm)	14.5
Compressed spring length: x_c (mm)	13.5
Ball diameter: D_b (mm)	13.05
Ball mass: m (gr)	8.9
Travel distance: x_L (mm)	30

The mechanical restoring force varies with the position of the ball as it moves along the tube according to the equation:

$$F_s(x) = \begin{cases} 0 & |x| \leq \frac{x_L}{2} - x_s \\ k_1(x - x_s) & \frac{x_L}{2} - x_s \leq |x| \leq \frac{x_L}{2} - x_c \\ k_1(x - x_s) + k_2(x - x_c) + \alpha(x - x_c)^3 & \frac{x_L}{2} - x_c \leq |x| \leq \frac{x_L}{2} \end{cases} \quad (5.2)$$

where x_s is the unstretched length of the springs, x_c is the fully compressed length of the springs, x_L is the track length, k_1 is the linear spring stiffness, k_2 the linear stiffness of the fully compressed spring, and α is the coefficient of cubic nonlinearity of the fully compressed spring. The travel distance is defined as the difference

between the track length and the ball diameter

$$x_L = x_t - D_b \tag{5.3}$$

The measured magnitudes of these parameters for the fabricated FDH prototype are listed in Table 5.2.

The electromagnetic restoring force for a given ball location x_i along the tube axis is obtained from FEM simulations of the FDH prototype with the ball placed at that location. The results are then fit into a second order polynomial

$$F_m(x) = \beta_\circ + \beta_1 x + \beta_2 x^2 \qquad -\frac{x_L}{2} x \leq \frac{x_L}{2} \tag{5.4}$$

to describe the variation of the electromagnetic restoring force as a function of ball position.

In the absence of the steel ball, the magnetic flux within the coil $\phi_\circ(x)$ is static. As the ball moves along the tube, it disrupts the magnetic field cutting the coil. Since the ball time constant, period of oscillation, is many orders of magnitude larger than the time constant of the electromagnetic field, we can adopt a quasi-static approach to field estimation. We calculate the magnetic flux within the coil $\phi_i(x_i)$ for a set of locations x_i by placing the ball at $x = x_i$ and using the FEM to determine the magnetic flux applied to the coil at that section. We then fit a two-dimensional function to describe the flux in the presence of the ball $\hat{\phi}(x)$.

The induced potential across the coil terminals occurs due to

$$\Phi(x) = \hat{\phi}(x) - \phi_\circ(x) \tag{5.5}$$

As the ball moves along the tube with a velocity of $\dot{x}$, the magnitude of the potential difference can be written as

$$V = -N \frac{\partial \Phi}{\partial x} \frac{\partial x}{\partial t} \tag{5.6}$$

where N is the number of coil turns. The electromagnetic force applied by the coil

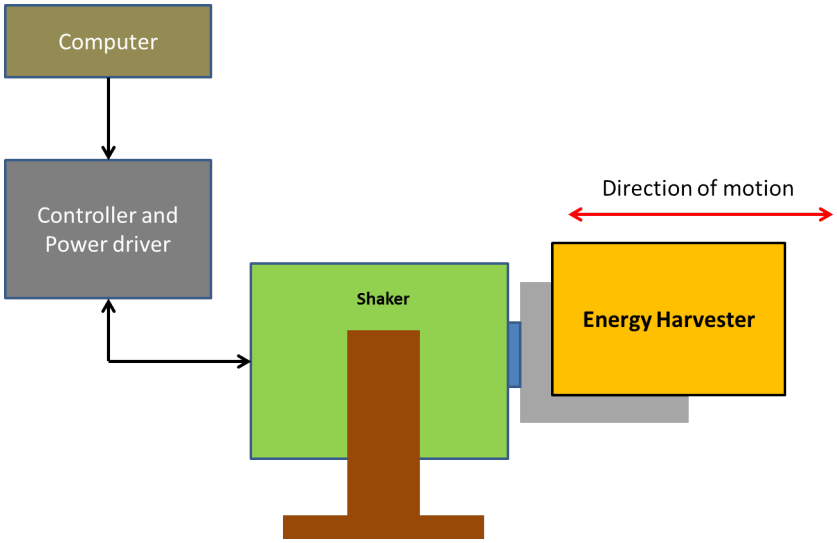

Figure 5.9: A schematic of the experimental Setup

on the ball F_m is described by Ampere's Law

$$c_e\dot{x} = -I\int_0^{2\pi} B \times dl \tag{5.7}$$

where B is the magnetic field intensity, l is the coil length, and I is the current in the coil. Using Ohm's Law, we can rewrite this equation as

$$c_e\dot{x} = -\frac{V}{R_p + R_L}\int_0^{2\pi} B \times dl \tag{5.8}$$

$$= \frac{N}{R_p + R_L}\frac{\partial\Phi}{\partial x}\dot{x}\int_0^{2\pi} B \times dl \tag{5.9}$$

where R_p is the parasitic resistance and R_L is the load resistance. Therefore, we obtain the electromagnetic damping coefficient as

$$c_e = \frac{N}{R_p + R_L}\frac{\partial\Phi}{\partial x}\int_0^{2\pi} B \times dl \tag{5.10}$$

5.4 Experimental results

The FDH was excited using an electromagnetic shaker and the RMS of its output voltage was recorded. The experimental setup is shown in figure 5.9. All experi-

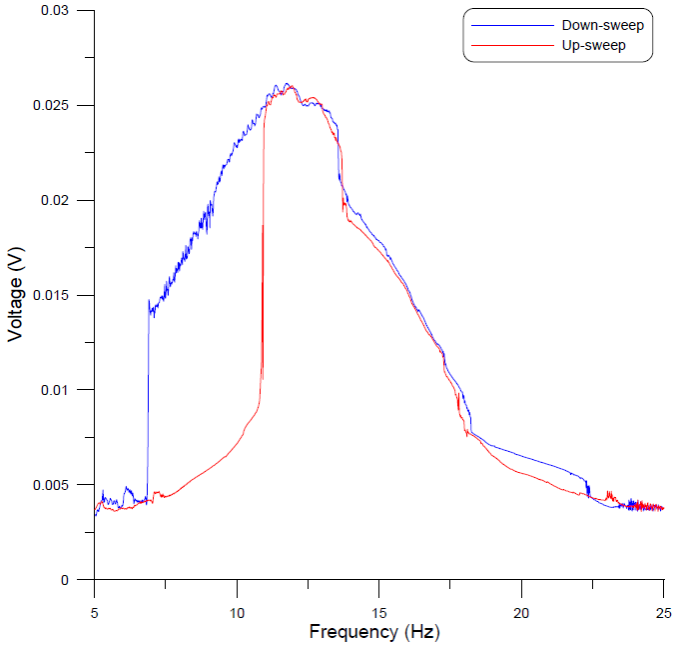

Figure 5.10: The open-loop frequency-output voltage curve of the FDH at base acceleration of $A = 0.9$ g

ments comprised of up and down frequency sweeps in the range of 5 to 25 Hz at a constant base acceleration with a slew rate of 5 Hz/min.

Table 5.3: FDH performance at four levels of base acceleration

Excitation amplitude (g)	$f_\circ$ (Hz)	Bandwidth (Hz)	Voltage (mV)
0.9	11.95	5.8	26
0.7	12.61	6.8	28.7
0.5	10.30	5.6	19.9
0.25	9.21	5.16	19.4

First, the FDH was tested in open-loop configuration with no load connected to it. Frequency sweeps were performed at base acceleration amplitudes ranging from 0.25 g to 0.9 g. Table 5.3 lists the center frequency $f_\circ$, harvesting bandwidth, and maximum output voltage for base accelerations of $A = 0.25, 0.5, 0.7$ and 0.9 g. The results show that the FDH is functional for a wide range of base accelerations. They also suggest that the FDH saturates around $A = 0.7$ g with the output voltage dropping and the harvesting bandwidth shrinking for higher base accelerations. The center frequency increases initially with base acceleration, which is expected as the

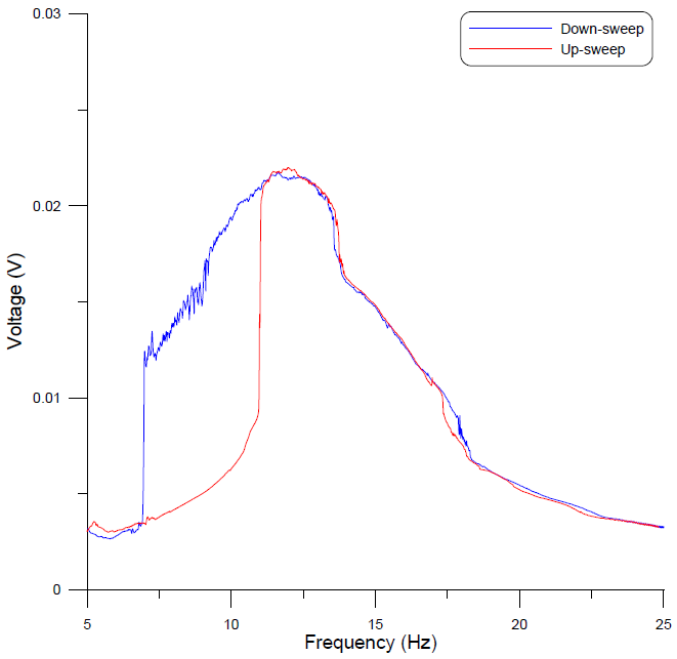

Figure 5.11: The frequency-output voltage curve of the FDH for a resistive load of 22.6 Ω and base acceleration of $A = 0.9$ g

ball spends more time in contact with end limiters, then drops beyond saturation level.

The frequency-output voltage (RMS) curve for a base acceleration of $A = 0.9$ g is shown in figure 5.10. Hysteresis is observed in the FDH response. During the up-sweep, the response jumps at a cyclic-fold bifurcation from a branch of small oscillations to a branch of large oscillations at 10.9 Hz. During the down-sweep, it jumps down from the large oscillation branch to the small oscillations branch at 6.9 Hz. The maximum output voltage realized is 26 mV at the FDH center frequency 11.95 Hz. The harvester bandwidth is calculated at 3db voltage from the maximum as 5.8 Hz. We note that while the FDH can harvest at the full bandwidth during a down-sweep, the bandwidth shrinks during an up-sweep due to hysteresis.

Repeating the experiment using a base acceleration amplitude of $A = 0.9$ g and attaching a resistive load of 22.6 Ω to the FDH, we obtained the frequency-output voltage curves shown in figure 5.11. The addition of the resistive load resulted in a drop in the maximum output voltage to 21.8 mV corresponding to an output power dissipated in the resistive load of 21.0 μWatt. Likewise the center frequency of the

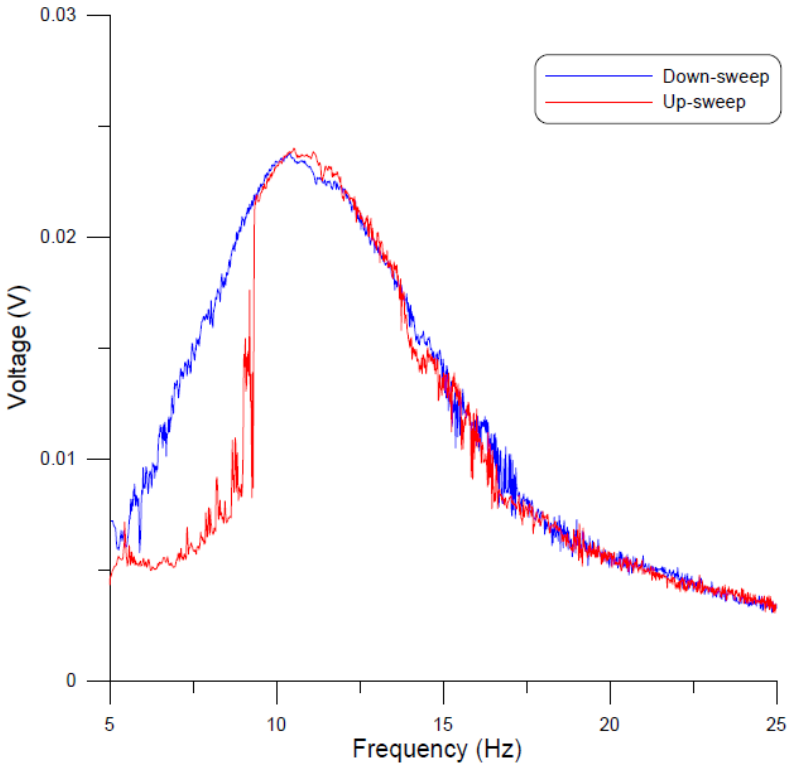

Figure 5.12: The frequency-output voltage curve of the FDH for a capacitive load of 1000 μF and base acceleration of $A = 0.9$ g

FDH dropped slightly to 11.61 Hz while the harvesting bandwidth was 6.23 Hz. It is interesting to note that the resistive load did not degrade the FDH performance from that of the open loop significantly.

Experiments were also conducted where the output load was changed from purely resistive to purely capacitive. Table 5.4 lists the center frequency, harvesting bandwidth, and maximum output voltage for capacitive loads of $0.1, 320$, and 1000 μF and a base acceleration of $A = 0.9$ g. While capacitive loads do not appear to change the maximum output voltage or the harvesting bandwidth, they do decrease the center frequency as the load capacitance increases.

Further, while capacitive loads do not necessarily change the characteristics of the FDH as seen from the frequency-output voltage of the 1000 μF load, Figure 5.12, they can be tuned to eliminate hysteresis from the frequency-output voltage as seen in the frequency-output voltage of the 0.1 μF load shown in Figure 5.13. This is an interesting result since it suggests the possibility of maintaining the same

Table 5.4: FDH performance for different types of loads

Load	$f_\circ$ (Hz)	Bandwidth (Hz)	Voltage (mV)
Open-loop	11.95	5.8	26
22.6 Ω (Optimal load)	11.6	6	21.7
1000 μF capacitor	10.52	5.88	24
320 μF capacitor	10.67	6.28	25
0.1 μF capacitor	11.61	6.23	24.3

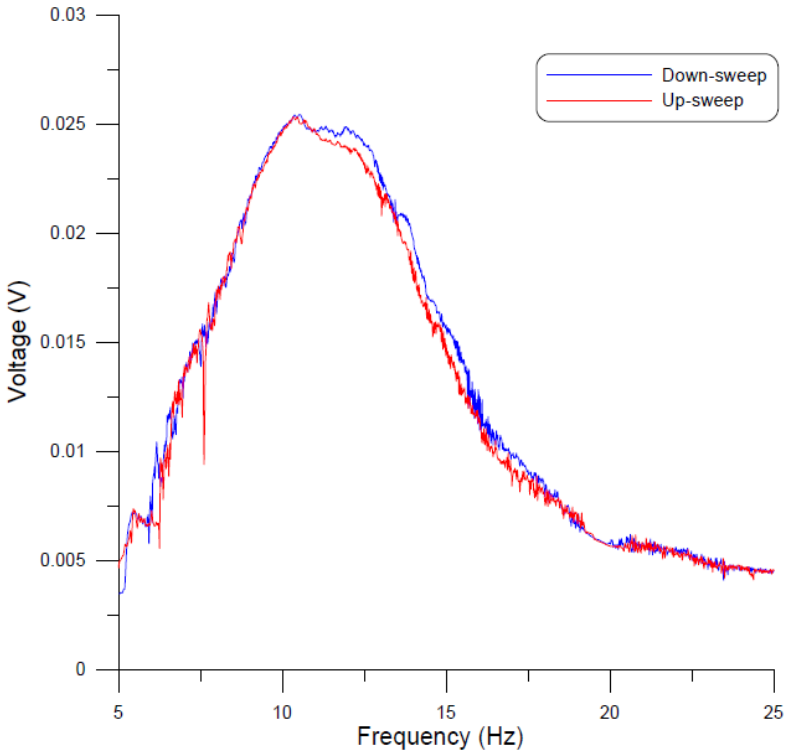

Figure 5.13: The frequency-output voltage curve of the FDH for a capacitive load of 0.1 μF and base acceleration of $A = 0.9$ g

wide harvesting bandwidth during up and down frequency sweeps.

5.5 Summary

In chapter five we introduced a new energy harvester design based on novel electromagnetic transduction mechanism by disrupting a static magnetic field, we called it "Field Disruption Harvester" (FDH), discussing the theory of operation, experimental results and introduced a mathematical model for the FDH, the design has

been tested under base accelerations of 0.25, 0.5, 0.7 and 0.9 g, and frequency up and down sweeps from 5 to 25 Hz. The harvester achieved a center frequency of between 10.5 and 12 Hz and harvesting bandwidth around 6 Hz. Where the frequency-output voltage response curve of the up-sweep experiments showed an interesting behavior that can be softening nonlinearity, while the down-sweep runs showed unknown dynamical behavior we could not analyze for the meanwhile. Changing the type of load connected to the FDH showed it can change the frequency-output voltage response significantly, increase or decrease FDH center frequency and harvesting bandwidth, where we can use improve the performance of the harvester.

Chapter 6

Conclusion

In this thesis we have discussed the basic concepts of energy harvesting from vibrations, parameters affect harvesting and design of electromagnetic based harvesters, also reviewed previous work of harvester designs using common mechanical structures, mass-on-spring and beam-support, and the usage of MEMS in harvesters design, compared the output power and natural frequency against each other.

In this chapter a design of a vibrations based energy harvester introduced, discussing the theory of operation, modeled and analyzed the response of a horizontally-aligned low-frequency springless vibration energy harvester. We tested the VEH experimentally and found that its response depends on the amplitude and frequency of base excitations. We also observed that as the base excitation was varied form 0.1 g to 0.4 g and the frequency was swept from 3 to 12 Hz. a consistent bending of the frequency response curves of the coil RMS voltage to the right indicating an effective hardening-type nonlinearity. The FFT spectrum of the seismic mass displacement shows the presence of both quadratic and cubic nonlinearities in the system response. The hardening cubic nonlinearity appears due to the end limiters configuration, while the dominant quadratic nonlinearity is driven by the electromagnetic coupling of the transducer (magnets and coil) to the impact oscillator motions.

In chapter four, we modeled and analyzed the response of a vertically-aligned low-frequency springless VEH. We tested the VEH experimentally and found that

its response contains three distinct regions of operation depending on the amplitude and frequency of base excitations. In all three regions, we observed a consistent bending of the frequency response curves of the coil RMS voltage to the left indicating an effective softening-type nonlinearity. The FFT spectrum of the seismic mass displacement shows the presence of both quadratic and cubic nonlinearities in the system response. The hardening cubic nonlinearity appears due to the end limiters configuration, while the dominant quadratic nonlinearity is driven by the electromagnetic coupling of the transducer (magnets and coil) to the impact oscillator motions. Further, the spring-type end-limiters were found to saturate the realizable output voltage to a maximum proportional to the track length but allow for a much wider energy harvesting bandwidth as the base excitations amplitude increases.

In chapter five we introduced a new energy harvester design based on novel electromagnetic transduction mechanism by disrupting a static magnetic field, we called it "Field Disruption Harvester" (FDH), discussing the theory of operation, experimental results and introduced a mathematical model for the FDH, the design has been tested under base accelerations of 0.25, 0.5, 0.7 and 0.9 g, and frequency up and down sweeps from 5 to 25 Hz. The harvester achieved a center frequency of between 10.5 and 12 Hz and harvesting bandwidth around 6 Hz. Where the frequency-output voltage response curve of the up-sweep experiments showed an interesting behavior that can be softening nonlinearity, while the down-sweep runs showed unknown dynamical behavior we could not analyze for the meanwhile. Changing the type of load connected to the FDH showed it can change the frequency-output voltage response significantly, increase or decrease FDH center frequency and harvesting bandwidth, where we can use improve the performance of the harvester.

6.1 Future work

The "Field Disruption Harvester" showed promising results and output in terms of low center frequency, wide harvesting bandwidth and relatively good output power

level that make it a successful candidate for various applications to power wireless sensor networks or portable devices from human locomotion, some experiments showed a significant change in the harvester frequency-output voltage response and harvesting bandwidth when changing the type of load connected to the FDH from purely resistive to purely capacitive load, where this change in response can be used to improve the performance of the FDH.

References

[1] P.D. Mitcheson, E.M. Yeatman, G.K. Rao, A.S. Holmes, and T.C. Green, "Energy Harvesting From Human and Machine Motion for Wireless Electronic Devices", *Proceedings of the IEEE*, Volume 96, no. 9, pp. 1457-1486, 2008.

[2] S. P. Beeby, M. J. Tudor, and N. M. White, "Energy harvesting vibration sources for microsystems applications", *Measurement Science and Technology*, Volume 17, no. 12, 2006.

[3] B.P. Mann, B.A. Owens, "Investigations of a nonlinear energy harvester with a bistable potential well", *Journal of Sound and Vibration*, Volume 329, Issue 9, pp. 1215-1226, 2010.

[4] R. Amirtharajah, A.P. Chandrakasan, "Self-powered signal processing using vibration-based power generation", *IEEE Journal of Solid-State Circuits*, Volume 33, no.5, pp.687-695, 1998.

[5] S. P. Beeby, R. N. Torah, M. J. Tudor, P. Glynne-Jones, T. O'Donnell, C. R. Saha, and S. Roy, "A micro electromagnetic generator for vibration energy harvesting", *Journal of Micromechanics and Microengineering*, Volume 17, no. 7, pp. 1257-1265, 2007.

[6] Ibrahim Sari, Tuna Balkan, Haluk Kulah, "An electromagnetic micro power generator for wideband environmental vibrations", *Sensors and Actuators A: Physical*, Volumes 145-146, pp. 405-413, 2008.

[7] Pei-Hong Wang, Xu-Han Dai, Dong-Ming Fang, Xiao-Lin Zhao, "Design, fabri-

cation and performance of a new vibration-based electromagnetic micro power generator", *Microelectronics Journal*, Volume 38, no. 12, pp. 1175-1180, 2007.

[8] M. A. E. Mahmoud, E. M. Abdel-Rahman, R. R. Mansour, and E. F. El-Saadany, "Springless Vibration Energy Harvesters", *ASME IDETC 2010*, Montreal, Canada, August 2010, DETC2010-29046.

[9] M. S. M. Soliman, E. M. Abdel-Rahman, E. F. El-Saadany, and R. R. Mansour, "Output Power Optimization for Electromagnetic Vibration Energy Harvesters", *ASME IDETC 2010*, Montreal, Canada, August 2010, DETC2010-28893.

[10] I. Khodadad, L. Ball, R. Baghat, I. Shafieloo, E. M. Abdel-Rahman, E. F. El-Saadany, and R. R. Mansour, A. Hajian, "Optimization of a Micro Power Uni", *ASME IDETC 2011*, Washington, DC, September 2011, DECT2011-48687.

[11] M. Bendame, K. Elrayes, E. M. Abdel-Rahman, M. A. E. Mahmoud, R. R. Mansour, and E. F. El-Saadany, "Vertically-Aligned Springless Energy Harvester", *ASME IDETC 2011*, Washington, DC, September 2011, DECT2011-48371.

[12] M. Bendame, K. Elrayes, E. M. Abdel-Rahman, M. A. E. Mahmoud, R. R. Mansour, and E. F. El-Saadany, "Horizontally-Aligned Springless Energy Harvester", *International Conference on Applied Mathematics, Modeling Computational Science*, Waterloo, Canada, July 2011.

[13] R. Keith Mobley, *Root cause failure analysis*, Butterworth-Heinemann, Oxford, UK, 1999.

[14] M. Raju, *Energy Harvesting, ULP meets energy harvesting: A game-changing combination for design engineers*, white paper, Texas Instruments, November 2008.

[15] http://encyclopedia2.thefreedictionary.com/charge+pump .

[16] http://www.electricityforum.com/products/trans-s.htm .

[17] http://www.understandingcalculus.com/chapters/11/11-4.php .